DOT/FAA/CT-82/20

Frictional Characteristics and Heat Transfer of Antimisting Fuel in Tubes

J. Wat
V. Sarohia

Prepared by
Jet Propulsion Laboratory
California Institute of Technology
Pasadena, California

August 1982

Final Report

Prepared for
Federal Aviation Administration, Department of Transportation
through an Agreement with
National Aeronautics and Space Administration

U.S. Department of Transportation
Federal Aviation Administration
Technical Center
Atlantic City Airport, N.J. 08405

TECHNICAL REPORT STANDARD TITLE PAGE

1. Report No. DOT/FAA/CT-82/20	2. Government Accession No.	3. Recipient's Catalog No.

4. Title and Subtitle
Frictional Characteristics and Heat Transfer of Antimisting Fuels in Tubes

5. Report Date
August 1982

6. Performing Organization Code

7. Author(s)
Joe Wat and V. Sarohia

8. Performing Organization Report No.
JPL Publication No. 82-53

9. Performing Organization Name and Address
JET PROPULSION LABORATORY
California Institute of Technology
4800 Oak Grove Drive
Pasadena, California 91109

10. Work Unit No.

11. Contract or Grant No.
DTFA03-80-A-00215

13. Type of Report and Period Covered
Final
August 1980 - September 1981

12. Sponsoring Agency Name and Address
U.S. Department of Transportation
Federal Aviation Administration Technical Center
Atlantic City, N.J. 08405

14. Sponsoring Agency Code

15. Supplementary Notes

16. Abstract

Experiments have been performed to determine the skin friction and heat transfer behavior of antimisting kerosene (AMK) in pipe flows. The additive used in the AMK was FM-9 developed by Imperial Chemical Industries. AMK has been developed as an aviation safety fuel to reduce post-crash fires. The principle aim of the present investigation was to determine the modification in flow and heat transfer behavior caused by the presence of the antimisting polymer additive in jet fuel.

The present study indicates that the AMK skin friction versus Reynolds number, or Nusselt number versus Reynolds number behavior, can be divided into three regions: (1) Newtonian laminar region, (2) shear-thickening transition region, and (3) drag-reducing turbulent region. At low flow rates, AMK has Newtonian behavior, i.e. constant viscosity. At a certain critical wall shear rate which depends on the fuel temperature and additive concentation, shear thickening occurs and causes a large increase in skin friction and heat transfer rates. In the third region, the skin friction and heat transfer rates drop rapidly and fall below the predicted Newtonian flow skin friction and heat transfer values; e.g., for 0.3 percent FM-9 AMK at a temperature of 20° C, these values coincide with Newtonian values at solvent Reynolds number, Re_S, equal to 2.2×10^4 and 1.0×10^4. Beyond these points, there is a reduction in skin friction and heat transfer rates.

17. Key Words (Selected by Author(s))	18. Distribution Statement
Aircraft Fires Antimisting Fuels Fuel Fires Heat Transfer and Skin Friction	

19. Security Classif. (of this report)	20. Security Classif. (of this page)	21. No. of Pages	22. Price
Unclassified	Unclassified	83	

HOW TO FILL OUT THE TECHNICAL REPORT STANDARD TITLE PAGE

Make items 1, 4, 5, 9, 12, and 13 agree with the corresponding information on the report cover. Use all capital letters for title (item 4). Leave items 2, 6, and 14 blank. Complete the remaining items as follows:

3. Recipient's Catalog No. Reserved for use by report recipients.

7. Author(s). Include corresponding information from the report cover. In addition, list the affiliation of an author if it differs from that of the performing organization.

8. Performing Organization Report No. Insert if performing organization wishes to assign this number.

10. Work Unit No. Use the agency-wide code (for example, 923-50-10-06-72), which uniquely identifies the work unit under which the work was authorized. Non-NASA performing organizations will leave this blank.

11. Insert the number of the contract or grant under which the report was prepared.

15. Supplementary Notes. Enter information not included elsewhere but useful, such as: Prepared in cooperation with... Translation of (or by)... Presented at conference of... To be published in...

16. Abstract. Include a brief (not to exceed 200 words) factual summary of the most significant information contained in the report. If possible, the abstract of a classified report should be unclassified. If the report contains a significant bibliography or literature survey, mention it here.

17. Key Words. Insert terms or short phrases selected by the author that identify the principal subjects covered in the report, and that are sufficiently specific and precise to be used for cataloging.

18. Distribution Statement. Enter one of the authorized statements used to denote releasability to the public or a limitation on dissemination for reasons other than security of defense information. Authorized statements are "Unclassified–Unlimited," "U. S. Government and Contractors only," "U. S. Government Agencies only," and "NASA and NASA Contractors only."

19. Security Classification (of report). NOTE: Reports carrying a security classification will require additional markings giving security and downgrading information as specified by the Security Requirements Checklist and the DoD Industrial Security Manual (DoD 5220.22-M).

20. Security Classification (of this page). NOTE: Because this page may be used in preparing announcements, bibliographies, and data banks, it should be unclassified if possible. If a classification is required, indicate separately the classification of the title and the abstract by following these items with either "(U)" for unclassified, or "(C)" or "(S)" as applicable for classified items.

21. No. of Pages. Insert the number of pages.

22. Price. Insert the price set by the Clearinghouse for Federal Scientific and Technical Information or the Government Printing Office, if known.

PREFACE

This report presents the results of one phase of research carried out at the Jet Propulsion Laboratory, California Institute of Technology, Contract NAS7-100, Task Order RD 152, Amendment 249-253, sponsored by the Department of Transportation, Federal Aviation Administration under Agreement No. DTFA03-80-A-00215. The authors extend their gratitude to Mr. Stephen Imbrogno, FAA Tech. Center, for many valuable technical suggestions throughout this program. The authors are grateful to Prof. R. Sabersky, and Mr. E. Matthys for technical advice. The assistance of Ms. A. Jakub, Mr. D. Khoe, Mr. G. Mullen, Mr. B. Green, and Mr. R. Smither is greatly appreciated for fabrication and assembly of equipment and help in acquiring experimental data.

TABLE OF CONTENTS

PAGE

FIGURE CAPTIONS

LIST OF TABLES

PAGE

NOMENCLATURE

Letter Symbols:

A_f	heating area between tube wall and fuel
C_p	specific heat
D	tube inside diameter
D_2	inside diameter of the outer shell of a concentric tube heat exchanger
D_1	outside diameter of the inner tube of a concentric tube heat exchanger
h	heat transfer coefficient
h_f	heat transfer coefficient between tube wall and fuel
h_w	heat transfer coefficient between tube wall and water
k	thermal conductivity
k, k'	consistency index
L	length
$\dot{m}$	mass flow rate
n, n'	flow behavior index
P	static pressure
p_h	hole pressure error
$\dot{q}$	heat transfer rate
r	radius
r_i	inside radius
r_m	mean radius
r_o	outside radius
T	temperature
T_b	bulk temperature
T_w	wall temperature

TW	water temperature
t	wall thickness
$U, \overline{U}$	average flow velocity
U_f	average overall heat transfer coefficient defined by $\dot{q}/A_f\Delta T_m$ (See Appendix A)
r, z	cylindrical coordinates

Greek Letters:

$\dot{\gamma}$	rate of shear
$\dot{\gamma}_w$	wall shear rate; 8U/D in laminar flow
$\dot{\gamma}_{w_{cr}}$	critical wall shear rate
Δ	incremental quantity
δ	ratio of velocity gradient at wall of a pipe for non-Newtonian fluid to velocity gradient for Newtonian fluid at same flow rate
$\bar{\eta}$	elongational viscosity
μ	viscosity
μ_a	apparent viscosity
μ_a	generalized apparent viscosity
μ_b	bulk temperature viscosity
$\bar{\mu}_{eff}$	average effective viscosity
μ_{eff}	effective viscosity; $\tau_w/\dot{\gamma}_w$
μ_o	zero shear (rate) viscosity
μ_w	wall temperature viscosity
ρ	density
τ	shear stress
τ_w	wall shear stress; $D\Delta P/4L$

Dimensionless Group:

C_f Friction Coefficient; $\frac{\tau_w}{\frac{1}{2}\rho\bar{U}^2}$

Nu Nusselt Number; $\frac{hD}{k}$

Pr Prandtl Number; $\frac{\mu C_p}{k}$

Re, Re_o Zero Shear Rate Reynolds Number; $\frac{\rho\bar{U}D}{\mu_o}$

Re' Generalized Reynolds Number; $\frac{D^{n'}-2\bar{U}^{2-n'}}{k'8^{n'-1}}$ (reference 4)

Re_s Solvent Reynolds Number; $\frac{\rho\bar{U}D}{\mu_{Jet\ A}}$

St Stanton Number; $\frac{h}{\rho UC_p}$

SUMMARY

Experiments have been performed to determine the skin friction and heat transfer behavior of antimisting kerosene (AMK) in pipe flows. The additive used in the AMK was FM-9 developed by Imperial Chemical Industries. AMK has been developed as an aviation safety fuel to reduce post-crash fires. The principle aim of the present investigation was to determine the modification in flow and heat transfer behavior caused by the presence of the antimisting polymer additive in jet fuel.

The apparatus used in this investigation was a concentric tube heat exchanger. Test sections 46 centimeters (cm) long of 321 commercially smooth stainless steel tube having inner diameters of 2.57 millimeters (mm) and 5.33 mm were used. Reynolds numbers between 10^2 to 5×10^4 were investigated. Tube Reynolds numbers in aircraft fuel systems can be as high as 10^4 to 10^5 under cruise and takeoff conditions. Pressure and temperature differentials across the tube were recorded. Measurements were performed with various FM-9 concentrations, levels of AMK restoration (degradation) and fuel temperatures (20° to 40° Centigrade). Visualization of the AMK flow at the end of the tube was undertaken to obtain qualitative information regarding the tube flow behavior, i.e. laminar, transitional or turbulent.

The present study indicates that the AMK skin friction versus Reynolds number, or Nusselt number versus Reynolds number behavior, can be divided into three regions: (1) Newtonian laminar region, (2) shear-thickening transition region, and (3) drag-reducing turbulent region. At low flow rates, AMK has Newtonian behavior, i.e. constant viscosity. At a certain critical wall shear rate which depends on the fuel temperature and additive concentration, shear thickening occurs and causes a large increase in skin friction and heat transfer rates. For some fluids such as 0.1 percent FM-9 AMK and partially

degraded AMK the second region is not observed. In the third region, the skin friction and heat transfer rates drop rapidly and fall below the predicted Newtonian flow skin friction and heat transfer value; e.g. for 0.3 percent FM-9 AMK at a temperature of 20° C, these values coincide with Newtonian values at solvent Reynolds number, Re_s, equal to 2.2×10^4 and 10^4. Beyond these points, there is a reduction in skin friction and heat transfer rates.

Since the critical wall shear rate is a function of the temperature, temperature changes in the fluid shift the shear-thickening transition region. This critical wall shear rate is approximately equal to 10^3 seconds $(s)^{-1}$ at a temperature of 20° C, and the corresponding critical solvent Reynolds numbers Re_s are 1.5×10^2, 6.0×10^2 and 2.0×10^3 for tube sizes equal to 1.00, 2.57 and 5.33 mm, respectively. With fuel hotter than room temperature (20° C) a delay of the transition phenomenon is observed. This implies that an increase in the critical wall shear rate follows an increase in the fuel temperature. Thus, a delay of the transition of AMK flow in tubes can result from heating the fuel.

In summation, however, it should be added that within the present experimental limits, there is some interesting flow behavior in the shear-induced transition region. From a design point of view FM-9 AMK does not drastically modify the frictional and heat transfer characteristics of the fuel.

1. INTRODUCTION

In aircraft fuel and engine systems, the size of the fuel lines range from 10 cm in diameter in the transfer pipes to approximately 2 mm diameter in fuel-oil heat exchangers in the engine. The Reynolds numbers in these lines can be as high as 10^4 to 10^5 at cruise or takeoff conditions. In order to avoid unexpected changes in pumping and heat transfer performance in both the aircraft and the engine fuel systems, a thorough study of pressure drop and heat transfer characteristics of AMK is necessary.

It is well known that AMK containing the FM-9 polymer additive shows non-Newtonian behavior at high shear rates (references 1,2). Previous work (references 2,3) has been done on the flow and heat transfer characteristics of this fluid in capillary flow. Shear thickening and degradation were observed.

AMK can be categorized as a time-dependent non-Newtonian fluid in which the polymer structure could be degraded by shear. However, by assuming laminar flow in which degradation of AMK is negligible, no slip on the wall, and $\dot{\gamma} = f(\tau)$ only, a generalized formulation (reference 4) for shear stress determined from tube viscometer data can be written as:

$$\tau = k \left(\frac{\partial U}{\partial r} \right)^n = k \dot{\gamma}^n \qquad 1.1$$

or

$$\tau_w = k' \dot{\gamma}_w^{n'} = k' \left(\frac{8U}{D} \right)^{n'} \qquad 1.1a$$

A larger value of k' implies a more viscous fluid while n' contains the physical properties of the fluid. Both k' and n' are functions of the temperature. Note that when the fluid is Newtonian, $k' = \mu$, $n' = 1$ and $\dot{\gamma}_w = 8\bar{U}/D$. For a shear-thinning pseudoplastic fluid, n' has a value less than 1, and for a shear-thickening fluid, n' has a value larger than 1.

For a non-Newtonian fluid, viscosity becomes a function of the shear rate. Thus, researchers have been using different definitions of viscosity in the equation for the Reynolds number. For example, Metzner and Reed (reference 5) suggested a generalized viscosity and Reynolds number:

$$\mu'_a = k' \left(\frac{8\bar{U}}{D}\right)^{n'-1} \tag{1.2}$$

$$Re' = \frac{\rho \bar{U} D}{\mu'_a} \tag{1.3}$$

Other researchers (reference 4) have used an apparent viscosity

$$\mu_a = \tau/\dot{\gamma} \quad \text{or} \quad \tau/\dot{\gamma}_w \tag{1.4}$$

or effective viscosity:

$$\bar{\mu}_{eff} = \frac{\tau_w}{8U/D} \tag{1.5}$$

where $8\,\bar{U}/D$ is the velocity gradient at the wall for a Newtonian laminar pipe flow. Zero shear rate viscosity, μ_o, is defined as the viscosity of the fluid at vanishingly small shear rate. In this study, prediction of pressure drop against mass flow rate is of primary interest. Therefore, besides μ_o (which has been proven to be equal to $\bar{\mu}_{eff}$ in our case), the solvent viscosity is also used for the Reynolds number. Hence, the solvent Reynolds number,

$$Re_s = \frac{\rho \bar{U} D}{\mu_{Jet\ A}} \tag{1.6}$$

and the Reynolds number,

$$Re = \frac{\rho \bar{U} D}{\mu_o} \tag{1.7}$$

are both used in our calculations.

For a Newtonian fluid, the correlation between the friction coefficient and Reynolds number is

$$C_f = \frac{16}{Re} \quad \text{(laminar pipe flow)} \tag{1.8}$$

and

$$C_f^{-1/2} = 4 \log (ReC_f^{1/2}) - 4 \qquad 1.9$$

(Prandtl-Karman turbulent pipe flow).

While the mechanism is not completely understood, drag reduction for non-Newtonian fluids in turbulent flow is commonly observed. In this study, data below the Prandtl-Karman curve in the turbulent region were found. The solvent Reynolds number beyond which drag reduction occurs is called the threshold Reynolds number. As reported in reference 6, viscosity has only a minor effect on the increase of the boundary sublayer thickness, assumed to be the main factor responsible for the drag reduction. Therefore, drag reduction in AMK is possible even though its shear free viscosity is approximately two times that of Jet A at room temperature. Thus, a C_f vs Re_s plot of the data will show whether a drag reduction will occur in an AMK pipe flow.

There are few experimental results on the heat transfer from non-Newtonian fluids. Turbulent heat transfer data are scarce because such flows are not encountered in the food industry where most of the non-Newtonian heat transfer studies are being done. However, information about the heat transfer coefficient, h_f, between a pipe wall and AMK flowing inside is required to provide information so that excessive heating of the fuel in fuel-lines can be avoided and also for the design of efficient fuel-oil heat exchangers in aircraft engine systems.

For a non-Newtonian fluid:

h_f = f (geometry of the surface, velocity and velocity gradient of the flow, physical properties of the fluid and fuel temperature gradient)

For laminar flow:

$$Nu = \frac{hD}{k} = Nu\ f\ (Re,\ Pr,\ D/L,\ \mu_b/\mu_w)$$

For turbulent flow:

$$Nu = Nu\ f\ (Re, Pr, \mu_b/\mu_w)$$

Sieder and Tate (reference 7) suggested empirical equations to correlate heat transfer data for liquids in pipe flow:

i) for laminar flow:

$$Nu = 1.86\ (RePrD/L)^{0.33}\ (\mu_b/\mu_w)^{0.14} \qquad 1.10$$

ii) for turbulent flow:

$$Nu = 0.023\ re^{0.8}\ Pr^{0.33}\ (\mu_b/\mu_w)^{0.14} \qquad 1.11$$

Medani and Hayes's work (reference 8) on AMK with 0.3 percent FM-4 additive proposed

$$Nu = 0.00165\ Re^{1.14}\ Pr^{0.33}\ (\mu_b/\mu_w)^{0.14} \qquad 1.12$$

Fiorentino, Desaro and Franz (reference 3) performed similar work with 0.3 percent FM-9 AMK. They both concluded that AMK has less heat transfer rate in high flow rates than Jet A.

Thermal properties of AMK, such as thermal conductivity and specific heat, are difficult to measure in the laboratory (see ASTM D2717 and D2766). Orr and Dallavalle's formula (reference 9) shows that the change of values in these thermal properties is small. Hence, values obtained from handbooks for kerosene (Jet A) are used in the present investigation. All dimensionless groups involved are calculated using the bulk temperatures measured directly in the experiments.

In this study, both skin friction coefficient and Nusselt number were obtained and plotted against the Reynolds number. In order to understand the rheological behavior of AMK, different parameters such as additive concentrations, tube sizes, and fuel temperatures were varied in the present experiments. Also, AMK samples of different degrees of degradation were used. Entrance effects on heat transfer characteristics of AMK pipe flows were also studied.

As mentioned earlier, AMK tends to degrade in high shear flow. Early in this effort, attempts were made to measure the degree of degradation at specific locations along the flow line of the experimental setup. This effort was abandoned later because of excess fuel consumption in the sampling process. However, samples taken from the receiving tank after specific experiments were tested using quality control methods, i.e. filter and cup tests, which are described in Appendix C.

Equations and physical constants utilized for calculations based on the heat transfer experimental data are shown in Appendix A.

2. EXPERIMENTAL APPARATUS, INSTRUMENTATION, AND TEST PROCEDURE:

2.1 SKIN FRICTION AND HEAT TRANSFER EXPERIMENTAL CONFIGURATIONS:

The schematic diagram of the experimental setup is shown in Figure 1. This setup can be subdivided into four sections as follows. Sections 2, 3 and 4 are shown in Figure 3.

Section 1: This section includes a fuel supply tank, a ball valve, an electric heater and a mixer. The 45 kilogram (kg) supply tank is adequate to handle fuel consumption rates as high as 0.25 kg/s for the duration of experiments needed to perform high Reynolds number experiments. The tank is installed sideways (see Figure 2), insuring a steady pressure head for experiments at high flow rates. A nitrogen drive system provides a tank pressure of up to 200 psig. An electric heater, controlled by a temperature controller, provides precise fuel temperature in the tank. A mixer composed of two large-opening (70% open) mesh wires installed perpendicular to the flow line is put one-half meter downstream of the ball valve and 25.4 mm upstream of the thermocouple providing a steady fuel temperature before section 2. All temperatures are measured with chromel-constantan thermocouples.

Section 2: A removable 0.5 m long insulated smooth stainless steel tube with a conical entrance is connected to section 1. This section ensures fully developed flow patterns in section 3. When section 2 is removed from the system, entrance effects on skin friction and heat transfer can be evaluated.

Section 3: Section 3 is the test section. Figure 3 shows the experimental setup for isothermal skin friction measurements. This section consists of a 70 cm long stainless steel test unit which uses the same size tubes as in section 2. A 60 cm stainless steel tube with a larger diameter connects the test unit to section 4. The temperature measurements are taken about 5 cm from the entrance of the larger tube. When fluid passes through the entrance

expansion of the larger tube, mixing occurs and provides uniform temperature fuel flow. The heat exchanger shell is built with 6.03 cm outside diameter (O.D.) steel pipe. The heat exchanger tube is 46 cm long. Heated water is supplied by a turbine-type pump which provides a constant flow rate, 0.76 kg/s, throughout the duration of the test. Eight Watlow band heaters and a temperature controller maintain the water temperature at 95° C ±2 during the heat transfer experiments. Fuel temperatures between 20° and 40° C were used in these experiments. Temperature differences between 5° and 40° C could be obtained, depending upon the flow rate. For example, at $Re_S \simeq 10^4$, the fuel temperature differences between the entrance and exit of the heat exchanger were usually only around 5° C. By contrast, temperature differences as high as 40° C were observed at laminar flow region, $Re_S < 2000$. A Fischer and Porter flowmeter is used for the measurement of water flow rates. Pressure transducers are used for the pressure differential measurements. In measuring static pressure of a non-Newtonian flow, errors due to the pressure hole (reference 10) are of the same order of magnitude as the normal stress. However, when a differential pressure transducer is used, assuming constant shear, constant bulk viscosity near the holes and constant velocity profile, the pressure error will be the same at both ends of the transducer. Using these assumptions, ΔP can be measured with a minimum of error. However, if fuel degrades between the measuring points the above argument is not true.

Section 4: A needle valve is installed to control the flow rate in this section. A gravimetric method is used to calculate the exact flow rates.

Three sets of tubing were used in the experiment. A detailed list of the tube sizes and lengths is listed in Appendix B. All pressure and temperature outputs are displayed on a digital voltmeter. In the heat transfer experiments an eight-channel strip chart is used to display and record the steady

state temperature outputs at different locations.

2.2 MEASUREMENTS:

The entire experimental setup, including the supply tank, is insulated. Flow rates are controlled both by the supply tank pressure and the needle valve located in section 4. For the isothermal cases, pressure drops between the test sections are recorded for different flow rates. For heat transfer experiments, measurements are taken after the system becomes thermally stable. These data include pressure drop, fuel temperature in the supply tank, and fuel and water temperatures at the entrance and exit points of the heat transfer section. Wall temperatures at the outside surface of the inner tube can be taken and used to calculate the heat transfer coefficient, h_f, directly.

Filter ratio, ICI cup, concentric cylinder Brookfield viscometer, and JPL-modified Flammability Comparison Test Apparatus (FCTA) test procedures are used as measures of degradation. Appendix C gives the detailed operating procedures of the filter and cup quality control methods. Samples taken before the experiment and from the receiving tanks after the experiment are used to determine the level of degradation. The samples are taken only at the highest flow rates to provide an indication of maximum degradation in the system. This condition can be achieved by setting the supply tank at 200 psig with needle valve fully opened. In present experiments, degradation may occur in tubes in sections 2 and 3, as well as in the two tube elbows upstream of the test section, three tube elbows downstream of the test section, one tube contraction, one tube expansion and one mixer. As mentioned earlier, no effort is made to measure each degradation separately. Table 1 shows the results of degradation tests.

TABLE 1. RESULTS OF THE ASSESSEMENT OF DEGRADATION IN THE HEAT TRANSFER EXPERIMENTS

DESCRIPTION	BEFORE EXPERIMENT[2]				AFTER EXPERIMENT[2]				
	TEMP (°C)	VISCOSITY (Brookfield) (CP)	FILTER RATIO	CUP FLOW (ml)	TEMP (°C)	VISCOSITY (Brookfield) (CP)	FILTER RATIO	CUP FLOW (ml)	Re
Jet A	490	1.65	1.00	7.9	490	1.65	1.00	7.9	
AMK, 0.3% FM-9, Std. Conditions[1]	-	2.69	19.77	3.0	-	2.51	13.08	5.2	2.11×10^4
AMK, 0.2% FM-9	-	2.27	19.91	5.0	-	2.08	9.42	7.3	2.82×10^4
AMK, 0.1% FM-9	-	1.85	18.04	7.2	-	1.87	8.91	7.6	3.37×10^4
AMK, 0.3% FM-9,with 2.57 mm I.D. tube	-	2.69	19.77	3.0	-	2.61	11.97	4.6	1.08×10^4
AMK, 0.3% FM-9, degraded 30 seconds	120	2.33	6.81	7.3	140	2.30	3.80	7.4	2.84×10^4
AMK, 0.3% FM-9, degraded 60 seconds	187	2.22	2.87	7.4	-	2.23	2.13	7.4	2.96×10^4
AMK, 0.3% FM-9, higher fuel temperature, 40° C	-	2.66	24.28	3.7	-	2.46	12.60	6.1	3.08×10^4
AMK, 0.3% FM-9, with curtailed entrance	-	2.79	22.98	3.0	-	2.49	11.19	5.4	1.93×10^4

[1] Undegraded, at ≈ 23° C, using 5.33 mm I.D. tube with full 58.4 cm entrance length

[2] Tests are done at room temperature (≈ 23° C)

After the completion of the experiment, nitrogen is used to flush the system to reduce the amount of leftover fluid in the system from previous experiments.

Solvent Reynolds numbers up to 2500 and 600 for Jet A and AMK, respectively, have been obtained utilizing a driving pressure of 200 psig when the smallest tube of 0.89 mm inside diameter (I.D.) is used. Since Reynolds numbers above 600 could not be obtained when using AMK in the present setup, both skin friction and heat transfer measurements on this capillary tube were abandoned.

3. EXPERIMENTAL RESULTS

Since AMK has non-Newtonian behavior under shear, different parameters which may affect skin friction and heat transfer characteristics in pipe flow were studied and will be discussed below.

3.1 SKIN FRICTION MEASUREMENT:

3.1.1 Comparison of Jet A and 0.3 percent FM-9 AMK

As a basic reference and comparison, skin friction measurements with water and Jet A as working fluids have been done with the 4.57 mm tube. Results are as expected and are shown in Figure 4. Using the same tube, the measurements have been repeated with 0.3 percent FM-9 AMK and are shown in Figure 4. The solvent Reynolds number, as defined previously, has been used in presenting the results in Figure 4.

Data in the laminar flow region show that AMK has higher values of friction coefficients than Jet A at the same Reynolds number. Thus, the apparent viscosity of AMK is always higher than Jet A in this region. The data in this region closely parallels the 16/Re curve. An apparent transition region starts at Re_s = 2000 and ends at Re_s = 3500. For Re_s greater than 3500, the skin friction coefficient decreases with increasing Reynolds number and falls under the Prandtl-Karman curve (as defined on page 3) at $Re_s = 1.8 \times 10^4$. Thus, drag reduction, as mentioned previously, does occur in AMK pipe flow. However, the increased friction coefficient at Re_s = 2000 is unusual. As discussed in reference 2, AMK rapidly increases its resistance to shear beyond certain critical strain rates. It is suspected that shear thickening at this point (Re_s = 2000 in this case) causes the unusual jump of skin friction behavior in this plot. It is also questionable whether or not a truly turbulent flow can be sustained after this jump because for $Re_s > 3500$, the skin fric-

tion curve is parallel to the 16/Re curve. Wall shear stresses and wall shear rates were calculated in order to understand the rheological behavior of the AMK. The straight line in Figure 5 is the least squares fit to the data points in the laminar region. Using equation 1.1a, it is found that

$$n' = 1.02$$
$$k' = 3.86 \text{ cp.}$$

This implies, assuming $n' = 1$, that the viscosity of AMK at shear rates less than $2 \times 10^3 \text{ s}^{-1}$ is 3.86 centipoise (cp) and has a slope of -1 for the laminar flow region in a log C_f vs log Re_s plot. Using equation 1.5, the average effective viscosity is calculated to be 3.30 cp. Note that equation 1.1a and 1.5 yield slightly different viscosities from the same experimental data.

The same experiment is performed with a tube having a slightly larger diameter, showing a change in $\bar{\mu}_{eff}$, from 3.30 to 2.69 cp. The results from this experiment are used as a reference in the following discussion and plotted in Figures 6 through 8. The difference in average effective viscosity, 3.30 to 2.69 cp., shows that the quality of the AMK, which can possibly be affected by the blending techniques, transportation and storage conditions, etc. may lead to inconsistency in the results.

A plot of C_f vs Re assuming $\bar{\mu} = 2.69$ cp. (Figure 8), shows the shift of the data plotted in Figure 6 to the left. This shows that AMK acts like a Newtonian fluid until the transition region begins.

3.1.2 Influence of FM-9 Concentration:

Since the concentration of the polymer additive has an important role in the non-Newtonian behavior of the solution (reference 11), both skin friction and heat transfer experiments were performed with 0.3, 0.2 and 0.1 percent concentrations of FM-9 in AMK.

In a drag-reducing polymer solution (reference 11) for a given tube diameter, maximum drag reduction occurs at an optimum polymer concentration. As the concentration is increased, the onset of drag reduction and the slope of the drag reduction curve decreases. No further increase of drag reduction occurs when the concentration of the polymer is higher than this optimum concentration. If the shear stress required for onset of friction reduction occurs in the laminar flow regime, transition delay will occur. Hence, a smooth curve will result, extending from the laminar flow region to the turbulent flow region.

Experimental results of skin friction for different FM-9 concentrations are plotted in Figures 6 through 8. As shown in Figure 6, the threshold Reynolds numbers (onset of drag reduction) for 0.3 and 0.2 percent FM-9 AMK are approximately equal to 2.3×10^4 and 2.0×10^4, respectively. For 0.1 percent FM-9 AMK, however, the transition delay is easily observed and it has a threshold Reynolds number (point A) earlier than those with 0.2 and 0.3 percent FM-9 AMK (points B and C).

Figure 7 shows the least squares fits to five sets of data in the laminar flow region. The power law for the non-Newtonian fluid, equation 1.1a, is used and the results are shown in this figure. The experimental results indicate fairly constant values for $\bar{\mu}_{eff}$ in all four AMK skin friction measurements. Note the difference between the two values for $\bar{\mu}_{eff}$ calculated for the two experiments with 0.3 percent FM-9 (see Figure 7) as discussed in the previous section.

Figure 8 is another C_f vs Re plot which shows all four sets of AMK data. In this plot, however, average effective viscosities obtained from the experimental data and equation 1.5 are used to calculate the flow Reynolds number. Because of the definition of $\bar{\mu}_{eff}$, data in the laminar flow region is forced

to collapse on the 16/Re curve. These curves clearly show the shift of the apparent transition region. Note that the plot (Figure 6) using Re_s cannot show the shift of the transition region directly. For AMK with 0.2 percent FM-9, the transition region is not as distinct as the one for the 0.3 percent FM-9 AMK. For 0.1 percent FM-9 AMK, as previously discussed, there is no obvious transition region at all.

For the 0.1 percent FM-9 AMK experiment, C_f increases for Re_s greater than 3×10^4. It is hypothesized that degradation at these flow rates might cause an increase in the friction coefficient. The filter test, using samples taken at these higher flow rates, did not show obvious degradation. As was the case in former experiments, the flow rate is limited by the maximum supply pressure of 200 psig in the storage tank, preventing investigation of this phenomenon at Reynolds numbers higher than 5×10^4.

3.1.3 Effect of Tube Size:

Hoyt (reference 6) pointed out that, for a fixed additive concentration, small diameters will yield a smaller threshold Reynolds number in a drag reduction pipe flow. For the experiment discussed in this section, measurements of the skin friction with different tube diameters were undertaken. Since a scaling law of non-Newtonian fluid has not been completely established, these experiments serve as an important step in understanding AMK flow behavior with different tube sizes. Results are plotted in Figures 9 through 11. Data of the capillary viscometer experiment (reference 2) are also included in these figures.

The relative transition flow regions appear at different locations for different diameters (Figure 9). Because shear rates are inversely proportional to the tube diameter and Reynolds numbers are directly proportional to the tube diameter, smaller sized tubes yield higher shear rates at a fixed

Reynolds number. Assuming that a specific shear rate causes shear thickening in AMK and that the onset of shear thickening triggers the transition flow, it can be concluded that AMK flows in a small tube will have an earlier transition. Peng's data (reference 2), using a 1 mm diameter tube, shows the earliest transition flow region, supporting this conclusion. In past experiments using 0.3 percent FM-9 AMK, the wall shear rate at the onset of transition flow has a value ranging from 10^3 to 1.7×10^3 s^{-1}.

Because the quality of AMK is different from batch to batch as measured by filter ratio and cup tests, one cannot define precisely the onset of a shear-thickening process here. However, a reasonable estimate of this onset shear rate is $\dot{\gamma}_w = 10^3$ s^{-1}. Note that this onset shear rate is different from the critical shear rate obtained from the cone and plate viscometer in reference 2.

In Figure 9, the data obtained from experiments with the 2.57 mm I.D. tube does have a smaller threshold Reynolds number than the data with the 5.33 mm tube as expected. The slopes of the curves which joined the data after the transition jump in Figure 9 have a value quite close to -1. One may suspect that shear thickening causes the jump and the flow becomes laminar afterwards. Further investigations have been performed to verify this hypothesis and will be discussed later.

Figure 10 shows the wall shear stress versus wall shear rate for three of the same tubes. For the experiment with D = 5.33 mm tube size, the data show that there is a slight shear thickening before the actual jump in the transition region. The validity of these data should be verified by further experimentation. Figure 11 shows the importance of the tube size on the average pressure drop versus mean flow speed. One should be aware that AMK degrades at high flow rates. Therefore, skin friction in the early part of the test

section will be different from the end part of the test section. Using equation 1.1a, data in Figure 10 yield values of n' = 1.01 for both experiments with tube sizes equal to 5.33 mm and 2.57 mm I.D.

3.1.4 Effect of AMK Degradation:

Intentional and unintentional degradation of AMK in the fuel and engine systems of an aircraft will change both flow and heat transfer behavior. To investigate the influence of degradation on AMK flow behavior, fixed amounts of 0.3 percent FM-9 AMK were put into a household blender under maximum blending speed for degradation purposes. In these experiments, AMK was blended for 30 and 60 seconds; filter ratios of 6.81 and 2.87 were obtained, respectively.

Degraded 30 and 60-second AMK have no obvious apparent transition region (Figure 12), yet behave quite differently from each other in the apparent turbulent flow region. AMK with 30-second degradation time exhibits transition delay, has a friction coefficient slightly below Prandtl-Karman Newtonian solvent curve, and possibly has a larger drag reduction (as compared to Newtonian fluids) beyond $Re_S = 2 \times 10^4$. AMK with 60-second degradation period surprisingly has higher friction coefficients than the Prandtl-Karman curve between $Re_S = 2 \times 10^3$ to 8×10^3. Beyond this point, drag reduction occurs in a fashion completely different from either undegraded or 30-second degraded AMK.

Considering that the characteristics of polymer pipe flow are mainly governed by the additive's molecular size (reference 14), one can assume that these three sets of data represent three different kinds of polymer solutions. Consequently, different kinds of flow behavior will occur. With this assumption, one should note the fact that different apparent polymer solutions can be obtained by degrading a given solution by different methods of degradation.

Wall shear stresses versus wall shear rates are plotted in Figure 13. Least squares fits of the data in the laminar flow region with equation 1.1a yields values of n' = 0.98 and 1.03 for 30-second and 60-second degraded AMK, respectively. This implies that the fluid in these two cases behaves like Newtonian fluids in the laminar flow region.

3.1.5 Effect of Fuel Temperature:

In equation 1.1, both n' and k' are functions of temperature (reference 4). This can be shown easily from a wall shear stress versus wall shear rate plot. According to previous experiments, it was first speculated that temperature should not have any effect on AMK in the Newtonian response region.

Measurements of skin friction with different fluid temperatures have been performed with results plotted in Figures 14 through 16. In Figure 14 where solvent Reynolds number is used, data obtained at higher temperatures shift to the right. Also, data in the laminar region fail to provide a constant effective viscosity. This implies that the fluid has non-Newtonian behavior at high temperatures in this region. This contradicted our speculation in previous paragraphs and Peng's experimental results (reference 2). However, since difficulties were found in the present setup in maintaining constant fuel temperature during experiments, no conclusion about the behavior of AMK in laminar pipe flow can be made here. The dotted lines in Figure 16 show the possible transition locations at three different temperatures. Data beyond the transition region almost collapse onto one single curve in this plot. Since fluid temperature effects the heat transfer of non-Newtonian fluid, skin friction measurements discussed here will be used to understand the heat transfer experimental data discussed later.

3.1.6 Discussion

Ram and Finkelstein (reference 14) added polyisobutylene to crude oil and kerosene to explore the correlations among pipe diameter, molecular weight, solvent viscosity and drag reduction. Their working parameters, such as experimental solvent, tube dimension and degradation behavior, are quite similar to those we have discussed previously. The FM-9 used in AMK has a much higher molecular weight, while the polyisobutylene used in reference 14 had a molecular weight of only 1.4 to 5.0 x 10^6. Different polymers exhibit different non-Newtonian behavior which is mainly governed by the molecular weight and molecular interactions in a given solvent.

For FM-9 AMK critical wall shear rate is defined as the wall shear rate at which shear thickening takes place. The typical rheological behavior of FM-9 AMK below and above this critical wall shear rate is Newtonian and non-Newtonian, respectively. This behavior is not unique in the polymer solution. For example, at certain composition, Poly(vinyl Alcohol)-borate complexes exhibit rheological behavior similar to AMK (reference 15). Values of the critical wall shear rate obtained from previous experiments are listed in Table 2. Note that the values of n' are fluctuating around 1.0 for different experiments. Since no efforts have been made to measure the actual velocity profile, the apparent viscosity, μ_a, could not be observed beyond the critical shear rate. Thus, the jump in the C_f vs. Re_s plot may be caused by a large difference between μ_a and $\mu_{jet\ A}$.

Several researchers have measured velocity in the turbulent flow region of the drag-reducing flow (references 16, 17, 18). Their work proved that Vick's elastic sublayer model (reference 19) can be used to explain the drag reduction of certain kinds of polymer solution. However, the mechanism of this model, which increases boundary sublayer thickness, has not been vali-

dated (references 6, 11). Since AMK has different non-Newtonian behavior than those in the references, it is of interest to measure the velocity profile of AMK turbulent flow and to correlate the results with Vick's model.

A flush-mounted skin friction measurement, e.g. a flush mount hot film probe, will indicate the difference in skin friction at different flow locations. Due to the non-Newtonian behavior of AMK, a definite value of the skin friction cannot be obtained from this kind of measurement. However, it can provide an indication of the changes in fluid behavior, i.e. the degree of degradation along a pipe flow line at a fixed flow rate. Also, degree of turbulence at different flow rates can be calculated from this data which is based on the heat transfer at the boundary sublayer at the surface of the probe. This technique may be used as a method of predicting and measuring the degradation of AMK pipe flow in future studies.

3.2 HEAT TRANSFER MEASUREMENTS

Heat transfer characteristics of non-Newtonian fluid pipe flow have been investigated both experimentally and analytically (references 20, 21) over a wide range of Reynolds numbers. These results, however, do not provide enough information to accurately predict non-Newtonian behavior, especially in the case of a time-dependent fluid such as AMK. Due to the unusual non-Newtonian behavior of AMK discussed previously, independent heat transfer tests are necessary.

3.2.1 Comparison of Jet A and 0.3 percent FM-9 AMK

Results of the heat transfer experiment with Jet A and 0.3 percent FM-9 AMK are plotted in Figure 17. The transition region is seen clearly in the plot. Two AMK heat transfer experiments are reported. The data for AMK show higher scattering than those for Jet A. Due to the fact that AMK behaves like

TABLE 2. CRITICAL WALL SHEAR RATES AND RHEOLOGICAL BEHAVIOR OF AMK

Discussion Sections	DESCRIPTION	n'	k' (cP)	τ_{W_c} (sec^{-1})
3.1.1	AMK, 0.3% FM-9	1.02	3.86	2×10^3
3.1.2	AMK, 0.3% FM-9	1.01	3.03	1×10^3
	AMK, 0.2% FM-9	0.99	2.05	7×10^2
	AMK, 0.1% FM-9	0.99	1.86	7×10^2
3.1.3	AMK, 0.3% FM-9, using 2.57 min I.D. tube	0.98	2.46	1×10^3
3.1.4	AMK, 0.3% FM-9, degraded 30 secs.	0.98	2.36	9×10^2
	AMK, 0.3% FM-9, degraded 60 secs.	1.03	1.76	9×10^2
3.1.5	AMK, 0.3% FM-9, high temperature (37° C)	-	-	9×10^2

*Household blender was used to degrade the AMK.

a Newtonian fluid until certain critical wall shear rates or flow rates, it follows that AMK should also have Newtonian heat transfer behavior before this critical wall shear rate. For the 5.33 mm I.D. tube, the Reynolds number (for all heat transfer tests, Re = Re_o while μ_o reported in reference 3 were used) at this shear rate is approximately 10^3. Assuming that the thermal properties, i.e. C_p, k, etc., of AMK are the same as Jet A, equation 1.10 shows that AMK will have a slight increase in heat transfer rates due to the increase in Prandtl number, i.e. the increase in viscosity.

AMK has a higher skin friction coefficient after the critical wall shear rate where shear thickening starts instead of being bound by the Prandtl-Karman curve. In the present heat transfer experiment, data (Figure 17) show an increase of heat transfer rates in the corresponding regions. The heat transfer rates drop suddenly at Re $\approx$ 6 x 10^3 and fall below the Newtonian (Jet A) curve. As discussed by Cho (reference 19) and Wells (reference 20), a drag-reducing fluid will have a lower heat transfer rate in the drag reduction area. Present results show similar drag and heat transfer reductions.

A hypothetical explanation of the data is that the apparent viscosity increases rapidly during the shear-thickening process resulting in an increase in Prandtl number. Thus, the heat transfer rate also increases during this process (see equations 1.10 and 1.11). Following this shear thickening process, the apparent viscosity, as the Reynolds number increases, appears to decrease and the flow becomes turbulent. A decrease in skin friction and heat transfer rate then occurs, causing the curve to intersect the Jet A curve and continue to drop with increasing flow rates. However, this hypothesis has not been verified experimentally.

3.2.2 Influence of FM-9 Concentration:

Results of heat transfer measurements for three AMK concentrations are

plotted in Figure 18. The data has a large scattering in the laminar flow region for the experiments with 0.2 and 0.1 percent FM-9 AMK. This phenomenon is different from that found in the skin friction measurements in which smooth data were obtained in the laminar flow region. Although AMK at different concentrations of FM-9 has Newtonian behavior at low flow rates, the heat transfer rates are not as steady as for Jet A.

In Figure 18, the unconventional jump between $1.5 \times 10^3 < Re < 7 \times 10^3$ is seen for 0.2 percent FM-9 AMK. After the sudden drop in heat transfer behavior at $Re = 7 \times 10^3$, data fall below the jet A data and are approximately parallel to the Jet A curve. For 0.1 percent AMK, no such jump was observed. A transition delay is shown clearly in the plot.

Note, in Figure 18, the jump and transition delay for 0.2 and 0.1 percent FM-9 AMK is around the same Reynolds numbers as for the skin friction case in Figure 6. The 0.1 percent AMK curve resembles most of the drag-reducing polymer behavior reported by other researches in the past.

3.2.3 Effect of Tube Size

Little research has been done on the diameter effects on heat transfer behavior for drag-reducing flows. Data with two different tube sizes are reported in Figure 19. Because of the limitation in the supply tank pressure, data cannot be obtained beyond the jump in Nusselt number for the smaller size tube, D = 2.57 mm. Thus, the scaling argument in reference 22 cannot be completed with the existing experimental data.

The following discussion is for the results from experiments using the smaller size tube, D = 2.57 cm. In the laminar region, data are close to the theoretical values predicted by equation 1.10. The equation

$$Nu = 2.34\ Re^{0.34}$$

is a good fit to the data. The curve joining these data lies below the curve

for the data with larger tube diameter as expected from equation 1.10. The results obtained from these measurements show an earlier transition in the small size tube. Large heat transfer coefficients beyond the critical point where shear-thickening starts are found. For the skin friction measurements with this tube size, data show an earlier transition and increase of skin friction coefficient. Although data beyond Re = 10^4 are not available, similar results of the sudden drop in Nusselt number at high Reynolds numbers are predicted. Data resemble the results obtained in the previous two sets of heat transfer experiments.

3.2.4 Effect of AMK Degradation

Effect of the restoration level (degradation) of AMK on the heat transfer behavior appears in Figure 20. For 30-second degraded AMK (filter ratio [FR] = 6.81), transition delay is observed and both drag and heat transfer reduction occur beyond Re = 2 x 10^3. Surprisingly, there is no obvious shear thickening and both the C_f and Nu values are always less than those of Jet A in the turbulent region. For the 60-second degraded AMK (FR = 2.87) (Figure 12) there is an apparent transition in the friction curve. Similarly, this phenomenon is observed in the heat transfer curve in Figure 20. Note the close match of the Reynolds numbers between the start and end points of this hump in Figures 12 and 20. One can conclude that for the 60-second degraded AMK shear thickening occurs in the experiment. Small humps were found in the experiments with 0.2 percent FM-9, 0.1 percent FM-9 and degraded AMK in the laminar flow region, at Re ≈ 400. At this point, no conclusion can be drawn on this behavior.

3.2.5 Effect of Fuel Temperature

For a given system, i.e. fixed tube size, polymer concentration, and de-

gradation level, the temperature difference between the water and the fuel is the most important parameter for the heat transfer behavior. The influence of fuel temperature on heat transfer behavior is shown in Figure 21 for AMK temperatures of 23° and 40° C. Fuel temperature of 40° C was chosen because this value is close to the fuel flash point, 37° C. Figure 21 shows a large scattering of data in the laminar flow region. This may be caused by the fluctuation of the fuel temperature since precise control is very difficult to achieve during the experimental period. The fuel temperature would usually fluctuate ±2° C in a five-minute time span. These variations have a large effect on the experimental results at low flow rates (see discussion in 3.1.5).

In the heat transfer measurements with a fuel temperature of 40° C, the transition region shifts as is the case in skin friction measurements. Although the transition is shifted, data in the turbulent region should fall on the same curve when Re is used instead of Re_s.

3.2.6 Measurement with the Entrance Effect

The laminar boundary layer thickness increases as the fluid flows downstream from the tube inlet and fills up the tube after a certain critical length, $(L/D)_{cr}$. The heat transfer coefficient at the inlet region (see Appendix B for the experimental dimensions) should vary with the distance from the inlet and have a larger value than in the fully-developed region. Non-dimensional entrance lengths, the ratio between the inlet tube length to the diameter at the entrance of the heat exchanger, of 110 and 14 are used in these measurements. Data shown in Figure 22 show less heat transfer in both laminar and turbulent regions for L/D = 14 as compared to L/D = 110. Rapid increases and decreases of heat transfer are found in the region just past the shear thickening.

3.2.7 Discussion

The heat transfer data correspond well with the skin friction data. For example, Figure 23 shows the results of the skin friction and heat transfer measurements with different FM-9 concentrations as a function of Reynolds number. In the laminar region, both results show that AMK behaves like a Newtonian fluid. The region with unusual increases in heat transfer corresponds to the same region with increases in skin friction. Heat transfer reduction in the presumed turbulent region also corresponds to the drag reduction region in the skin friction measurements. Unfortunately, not enough data has been obtained in the turbulent region to allow detailed theoretical analysis of the correlation between momentum and heat transfer and should be further researched.

As mentioned earlier, there is uncertainty about the actual flow condition in the region beyond the flow transition region (or shear thickening region of AMK). By examining the data carefully, one can see that most of the heat transfer coefficients data after this transition region fall on a curve which is approximately parallel to the Jet A curve. Hence, it is concluded that turbulent flow is obtained in this region. According to the discussions in references 6, 12 and 13, the laminar sublayer in this region may be increased by the interaction between the polymer and the solvent, and both drag and heat transfer are reduced.

3.3 RESULTS OF THE DEGRADATION TEST

Degradation tests which include filter tests with a 20 μm polycarbonate filter, British cup test, viscosity measurements with Brookfield viscometer and fire test with FAA flammability test rig are done with samples taken before and after experiments. In heat transfer experiments, bulk temperature increases are only of the order of 5 degrees at this highest experimental flow

rate (about $Re_s = 3.0 \times 10^4$) at which a sample is taken. Because degradation tests with samples taken from skin friction measurements are incomplete, only results with heat transfer test samples are reported. Data are listed in Table 1.

All tests show obvious degradation of the fuel during the experimental process. When a tube section 50 cm long (the total length for a standard test is 125 cm) is removed in the entrance effect experiment (section 3.2.6), no obvious increases in degradation of fuel are observed. Therefore, the degradation of the fuel must be caused mostly by other components in the present experimental setup, e.g. the valve, as mentioned earlier.

Thus, the results from these kinds of degradation tests provide an incomplete understanding of flow degradation. One reason is that the shear strain rates for turbulent flows are unpredictable due to the non-Newtonian behavior of AMK.

The elongational viscosity, defined as

$$\bar{\eta} = \frac{\tau_{zz} - \tau_{rr}}{dV_z/dz}$$

in cylindrical coordinates, is claimed to be important in the drag reduction, gel formation and degradation of the polymer solutions. The end effects (reference 23) and the flow contractions and expansions in the experimental setup may cause a large elongational stress in the flow, resulting in higher degrees of degradation. At this point, the importance and mechanisms of these kinds of degradation are not well understood and need further research.

3.4 FREE-JET FLOW VISUALIZATION

The behavior of friction coefficient vs. Re curve for Newtonian fluids is well documented and leaves little doubt on the state of the fluid (laminar, transition, turbulent) as a function of flow rate (Figure 4). The curves for

non-Newtonian fluids, however, do not present such a clear understanding of their behaviors. For AMK, one sees that for low Reynolds numbers the behavior follows closely that of Jet A. The flow for both fluids is laminar in this region, as concluded earlier. However, in the turbulent region (for Re > 5 x 10^3) the behavior of AMK is quite different from that of Jet A. The slope of the curve for AMK in this region is much steeper than that of turbulent Jet A. In addition, this slope approximates that of the laminar AMK curve. The question is whether the AMK is turbulent or laminar in this region.

Preliminary experiments were performed to observe visually the behavior of AMK as a function of flow rate and to compare it with the behavior of Jet A. Within the range of Re which represents the transition region, the flow of Jet A is unstable and cannot be categorized readily as being laminar or turbulent (Figure 24a). At approximately the same Re, AMK appears to exhibit laminar flow (Figure 24b). Figures 25a and 25b show Jet A at Re = 5.31 x 10^3 and AMK at Re = 5.22 x 10^3. Flow patterns are quite similar to those of Figure 24.

In Figure 26a, Jet A at Re = 3.5 x 10^4 is clearly turbulent. In Figure 26b AMK at Re = 3.03 x 10^4 is shown. It is quite clear that the presence of polymer in Jet A significantly suppresses the jet turbulence (Figure 26b) as compared to Jet A (Figure 26a).

3.5 ADDITIONAL HEAT TRANSFER MEASUREMENTS:

In the original experimental setup, bulk water temperatures were measured at the entrance and exit points of the heat exchanger. This kind of measurement provides insufficient information since the wall temperature of the inner tube is not known. Therefore h_f cannot be obtained directly from the experimental data and consequently values of h_w in equation A.4 in Appendix A are

basically unknown. Although values of h_w can be obtained using equation A.5, these values must first be verified.

At a flow rate of 0.76 kg/s, equation A.5 yields values of h_w = 640 and 775 kg-cal/hrm° C for 5.33 and 2.57 mm I.D. stainless steel smooth tubes, respectively. In order to avoid the uncertainty in calculating h_w, wall temperatures were measured directly. The h_f can be calculated directly from this kind of measurement as discussed in Appendix A. Both Jet A and 0.3 percent FM-9 AMK were used in this experiment. The experiments were performed using the 5.33 mm tube. Results are plotted in Figures 27 and 28.

In Figure 27, Jet A data obtained without wall temperature measurements are also plotted. Since wall temperatures were unknown for these tests, the average value of μ_b/μ_w calculated from the experiment with wall temperature measurements is used. By comparing both sets of Jet A results, some deviation in the laminar region is evident. However, data in the transition and turbulent regions correlate well in both cases. Thus, data in these regions can be used to calibrate h_w by using equation A.4. Values of U_f from experiments without wall temperature measurements are used in this equation, along with values of h_f from experiments with wall temperature measurements. The h_w is found to be on the order of 6.2×10^2 kg-cal/hrm° C, which is close to the value from equation A.5. Hence, values of h_w obtained using equation A.5 are confirmed by this result.

Figure 28 shows that data of 0.3 percent FM-9 AMK collapse onto Sieder & Tate's curve in the laminar flow region and show shear thickening at the same Re for water temperatures of 85° and 95° C. In these experiments, AMK was kept at room temperature, 20° to 25° C, before entering the heat exchanger. The jump in this shear-thickening region is not as large as those in experiments discussed in previous sections.

In conclusion, heat transfer experiments without wall temperature measurements yield reasonable results, but can be improved by these measurements.

4. CONCLUSIONS

The modification in friction and heat transfer characteristics between AMK and Jet A, the subject of the present investigation, is of great importance in the design of the aircraft and engine fuel systems, particularly in the considerations of tube size, allowable line pressure drops, and the fuel-oil cooler heat-exchanger effectiveness. The key results of this investigation are as follows:

(1) For low AMK flow rates in small tubes up to about 5 mm diameter, in which the Reynolds number is less than about 2000, with various FM-9 concentrations, degrees of degradation, and fuel temperatures, AMK behaves like a Newtonian fluid. Thus, at flow rates which correspond to the laminar flow region, AMK is believed to have a constant viscosity. In this flow region skin friction and heat transfer behavior can be predicted by conventional Newtonian theory.

(2) At a certain critical wall shear rate, which is a function of the temperature, apparent transition of the flow occurs. This is believed to be caused by shear thickening. This shear-thickening process results in an increase in skin friction coefficient and Nusselt number. This critical wall shear rate will correspond to different Reynolds numbers for different size tubes. Hence, the apparent transition of the flow will be shifted laterally by changing the tube size. A larger tube will yield a transition at a larger Reynolds number. For 0.3 percent FM-9 AMK, e.g. this critical wall shear rate is roughly equal to 10^3 s^{-1}, and the corresponding solvent Reynolds numbers Re_s are 1.5×10^2, 6.0×10^2 and 2.0×10^3 for tube sizes equal to 1.00, 2.57 and 5.33 mm respectively.

(3) With increasing values of Reynolds numbers beyond the transition region, this shear-thickening process is followed by a decrease of skin friction

coefficient and Nusselt number. The skin friction coefficient and Nusselt number versus Reynolds number curves ultimately intersect the turbulent flow Newtonian (Jet A) curves. Reductions in the skin friction coefficient and Nusselt numbers occur beyond this point.

(4) Although viscosity, filter and cup tests yield expected results with AMK at different degrees of degradation, unexpected results were found in both skin friction and heat transfer measurements for degraded fuels. It appeared that shear thickening occurred in degraded AMK with a filter ratio of 2.87 (blended for 60 seconds) but not with degraded AMK of FR = 6.81 (blended for 30 seconds). These unexpected results do not support the assumption that longer degradation times imply behavior characteristics which approach those of Jet A. While this may be true for degradation measurements (viscosity measurement, filter test, cup test and flammability test), it may not apply to skin friction and heat transfer characteristics. The flow behavior of any polymer solution is governed by the polymer, the solvent, and their mutual interaction. Different apparent polymer solutions can be obtained by degrading a given solution by different methods of degradation. Thus, unless the degradation mechanisms and polymer interactions are known, the flow and heat transfer behavior of degraded fuel is in general unpredictable.

(5) Although no mathematical calculations were performed, by comparing the experimental data, skin friction and heat transfer measurements correlate well with each other in their behavior at different Reynolds numbers. Hence, isothermal flow tests (skin friction measurements) may be used to predict heat transfer behavior qualitatively.

REFERENCES

1. Sarohia, V., "Fundamental Studies of Antimisting Fuels", AIAA-81-1422, July 1981.

2. Peng, S., and Landel, R. F., "Rheological Behavior of a Progressively Shear Thickening Solution", Presented at the March Meeting of the American Physical Society, March 23-27, 1981.

3. Fiorentino, A., DeSaro, R. and Franz, T., "An Assessment of the Use of Antimisting Fuel in Turbofan Engines", NASA-CR-165258, Dec., 1980.

4. Wilkinson, W. L., "Non-Newtonian Fluids", Pergamon Press, 1960.

5. Metzner, A. B. and Reed, J. C., "Flow of Non-Newtonian Fluids - Correlation of the Laminar, Transition, and Turbulent-Flow Regions", A.I.Ch.E. Journal, Dec. 1955.

6. Hoyt, J. W., "The Effect of Additives on Fluid Friction", Transaction of ASME, June 1972.

7. Sieder, E. N. and Tate, G. E., "Heat Transfer and Pressure Drop of Liquids in Tube", Industrial and Engineering Chemistry, V. 28, No. 12, Dec. 1936.

8. Medani, M. s. and Hayes, K. G., "Heat Transfer to Aviation Fuels", Journal of Engineering Science, Vol. 4, No. 1, 1978.

9. Orr, C. and Dallavalle, J. M., "Heat Transfer Properties of Liquid Suspensions", Chem. Engng. Progr. Symposium Service No. 9, 50, 29, 1954.

10. Higashitan, K. and Lodge, A. S., "Hole Pressure Error Measurement in Pressure-Generated Shear Flow", Trans. of Society of Rheology, 19:2, pp. 307-335, 1975.

11. Gadd, G. E., "Friction Reduction", Encycl. Polym. Sci. Tech., 15, 224-253, 1971.

12. Seyer, F. A. and Metzner, A. B., "Turbulent Flow Properties of Viscoelastic Fluids", The Canadian Journal of Chemical Engineering, Vol. 45, June 1967.

13. Astarita, G., "Possible Interpretation of the Mechanism of Drag Reduction in Viscoelastic Liquids", I & E.C. Fundamentals, Vol. 4, No. 3, August 1965.

14. Ram, A., Finkelstein, E. and Elata, C., "Reduction of Friction in Oil Pipelines by Polymer Additives", Israel Journal of Technology, Vol. 6, No. 3, July 1967.

15. Savins, J. G., "Drag Reduction Characteristics of Solutions of Macromolecules in Turbulent Pipe Flow", Society of Petroleum Engineering Journal, Vol. 4, p. 203, 1964.

16. Reischman, M. M. and Tiederman, W. G., "Laser-Doppler Anemometer Measurement in Drag Reducing Channel Flow", J. Fluid Mech., Vol. 70, Part 2, pp. 369-392, 1975.

17. Elata, C., Lehrer, J., and Kahanovitz, A., "Turbulent Shear Flow of Polymer Solution", Israel Journal of Technology, Vol. 4, p. 87, 1966.

18. Bogue, D. C. and Metzner, A. B., "Velocity Profile in Turbulence Pipe Flow, Newtonian and Non-Newtonian Fluids", I & EC Fundamentals, Vol. 2, p. 143, 1963.

19. Vick, P.S., "An Elastic Sublayer Model for Drag Reduction by Dilute Solutions of Linear Macromolecules", J.Fluid Mech., Vol. 45, part 3, pp.417-440, 1971.

20. Cho, Y. I. and Hartnett, J. P., "Non-Newtonian Fluids in Pipe Flow", Advance in Heat Transfer, Academic Press, Vol. 15, 1981.

21. Wells, C. S., "Turbulent Heat Transfer in Drag Reducing Fluids", AIChE Journal, Vol. 14, No. 3, 1968.

22. Taylor, D. D. and Sabersky, R. H., "Extrapolation to Various Tube Diameters of Experimental Data Taken with Dilute Polymer Solution in a Smooth Tube", Letters in Heat and Mass Transfer, Vol. 1, pp. 103-108, 1974.

23. Bagley, E. B., "End Corrections in the Capillary Flow of Polyethylene", J. Applied Physics, Vol. 28, No. 5, p. 624, 1957.

24. Davis, E., "Heat Transfer and Pressure Drop in Annuli", Trans Am. Soc. Mech. Engr., 65, p. 755, 1943.

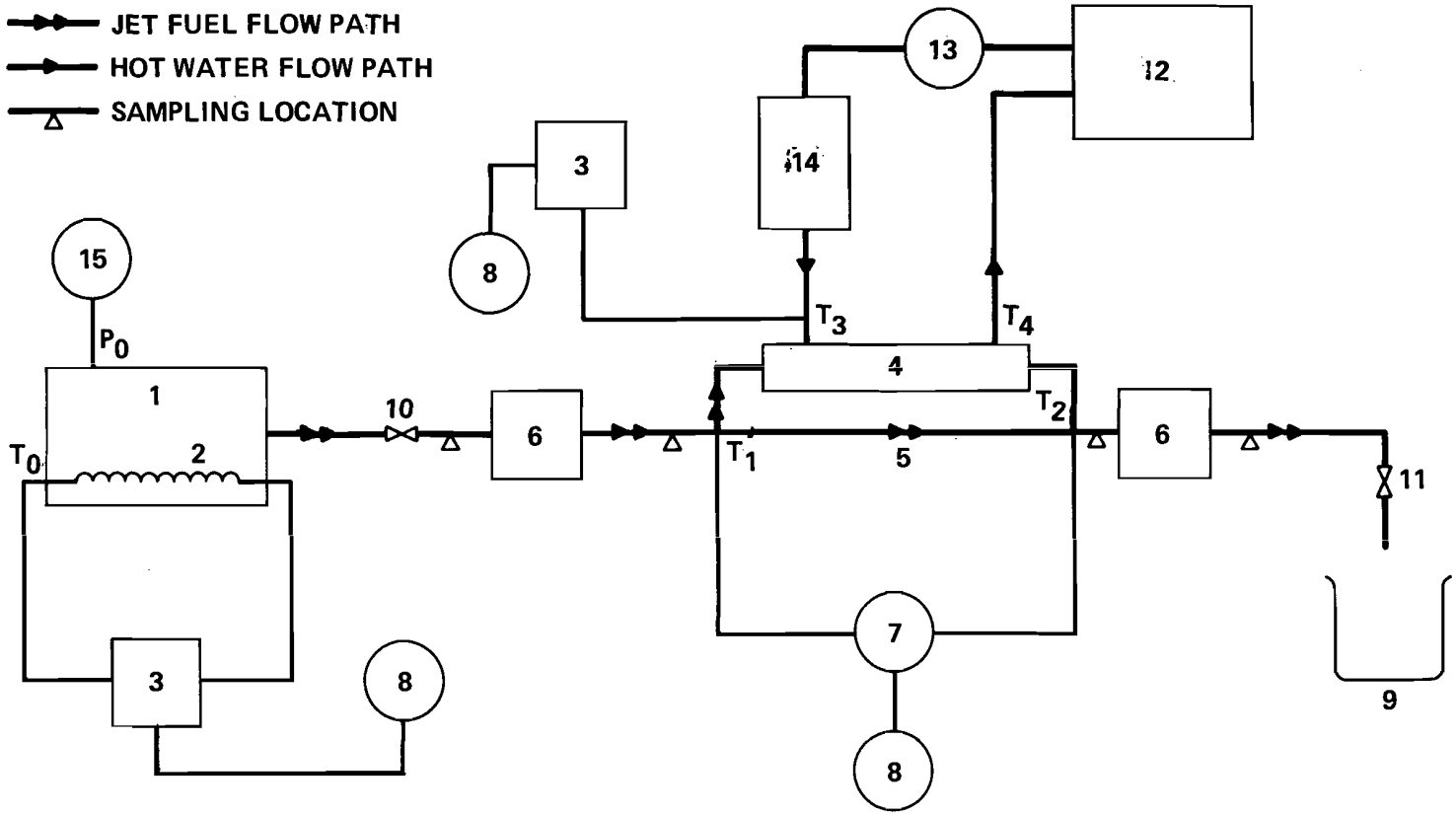

1. FUEL TANK (15 gal.)
2. HEATER
3. TEMPERATURE CONTROLLER
4. CONCENTRIC HEAT EXCHANGER
5. ALTERNATE TEST SECTION (FOR SKIN FRICTION)
6. MIXER
7. PRESSURE TRANSDUCER
8. DVM
9. RECEIVING TANK
10. BALL VALVE
11. NEEDLE VALVE
12. WATER TANK (WITH PUMP)
13. FLOW METER
14. HEATER
15. NITROGEN SUPPLY

FIGURE 1. SCHEMATIC DIAGRAM OF APPARATUS FOR SKIN FRICTION AND HEAT TRANSFER MEASUREMENT

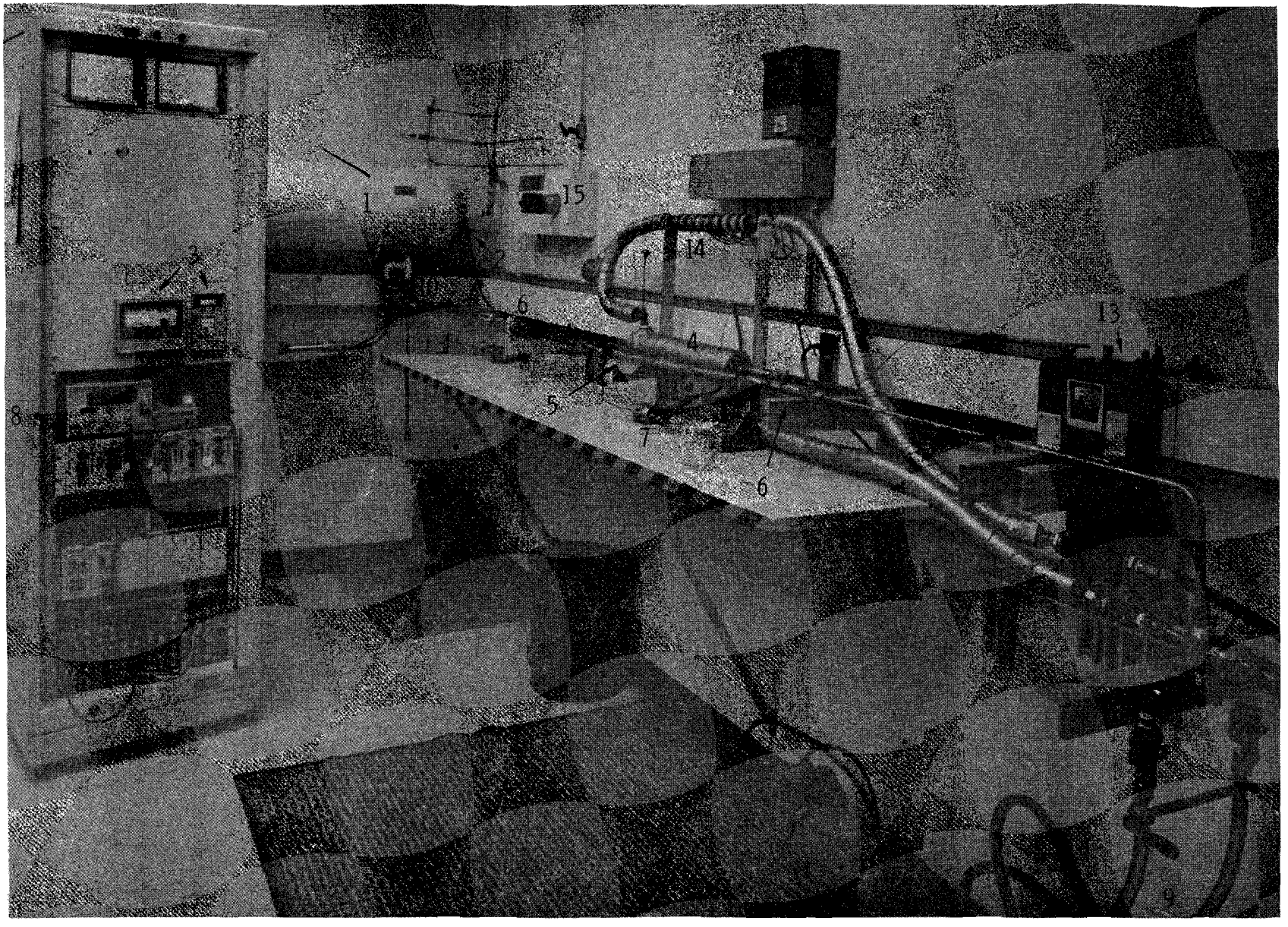

FIGURE 2 EXPERIMENTAL ARRANGEMENTS

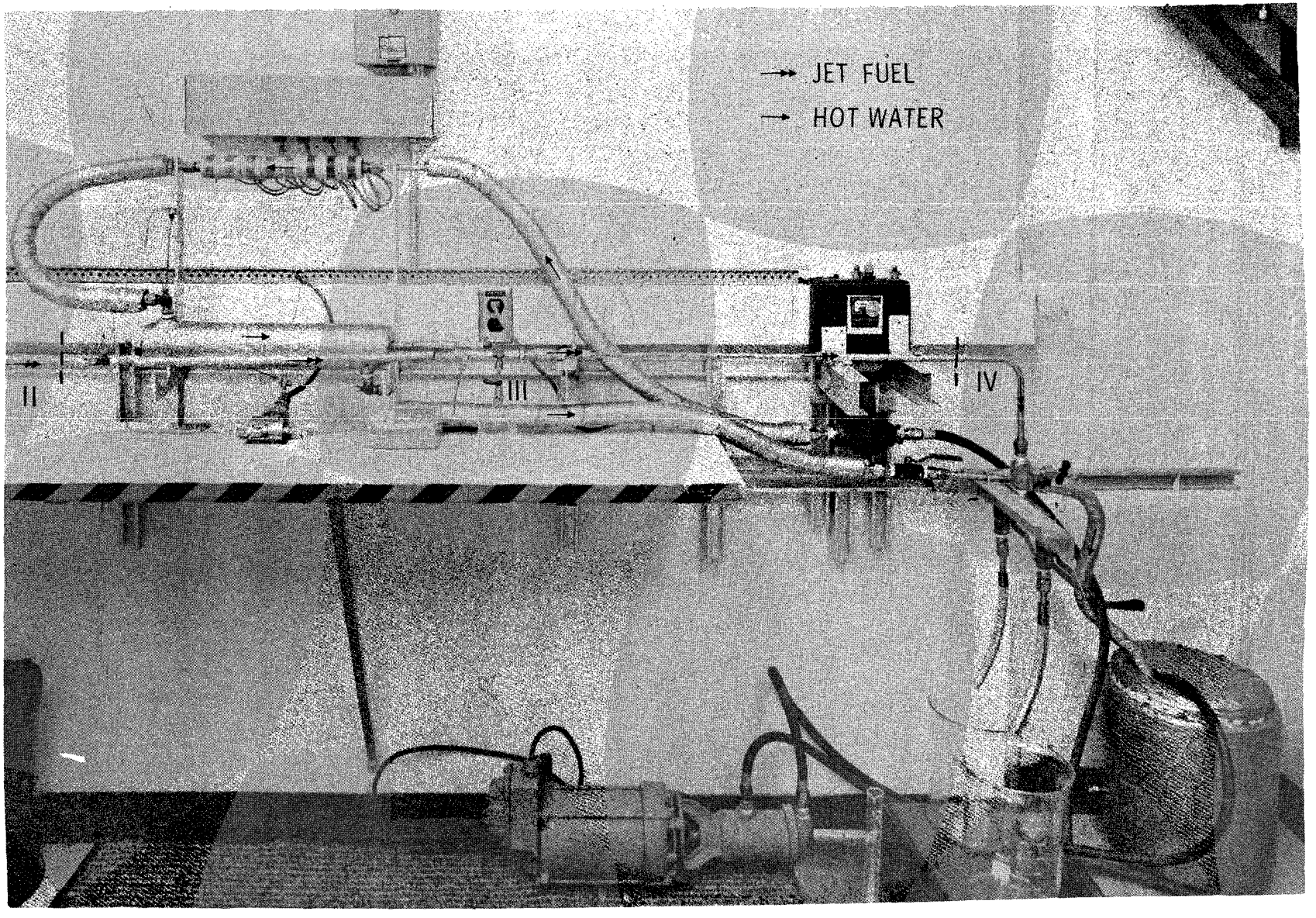

FIGURE 3 TEST SECTIONS OF SKIN FRICTION AND HEAT TRANSFER MEASUREMENT

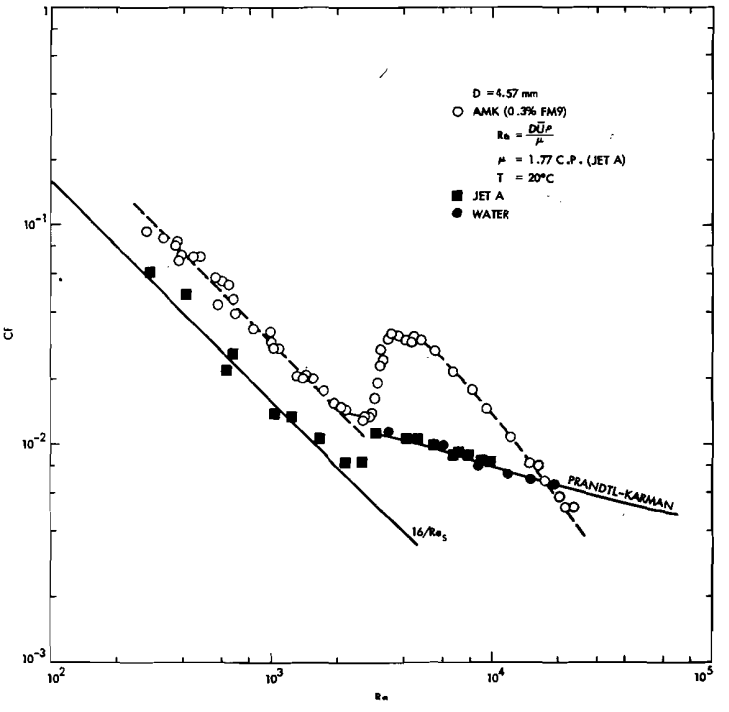

FIGURE 4. COMPARISON BETWEEN JET A AND 0.3% FM-9 AMK, D = 4.57 MM, $\mu = {}^{\mu}$JET A

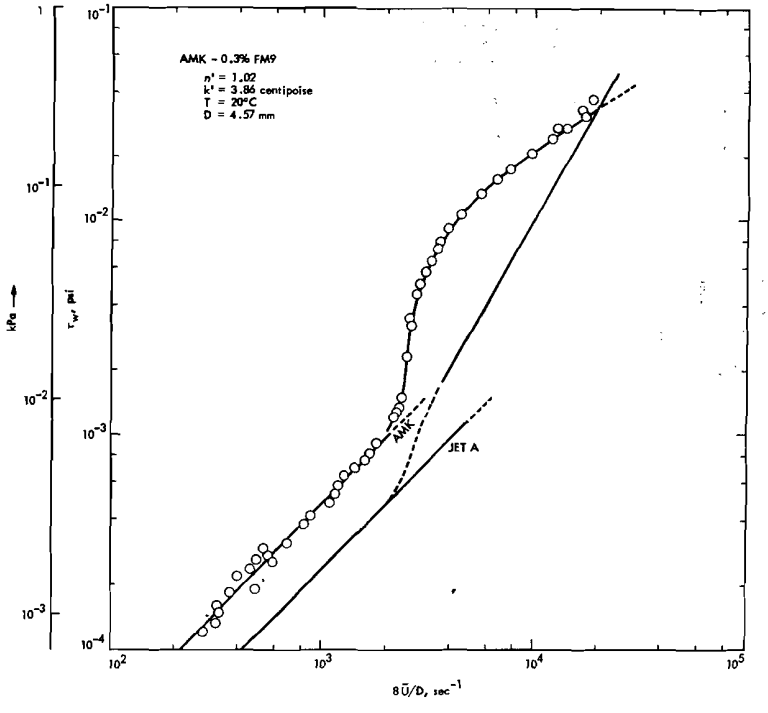

FIGURE 5. COMPARISON BETWEEN JET A AND 0.3% FM-9 AMK; τ_w vs. $\dot{\gamma}_w$

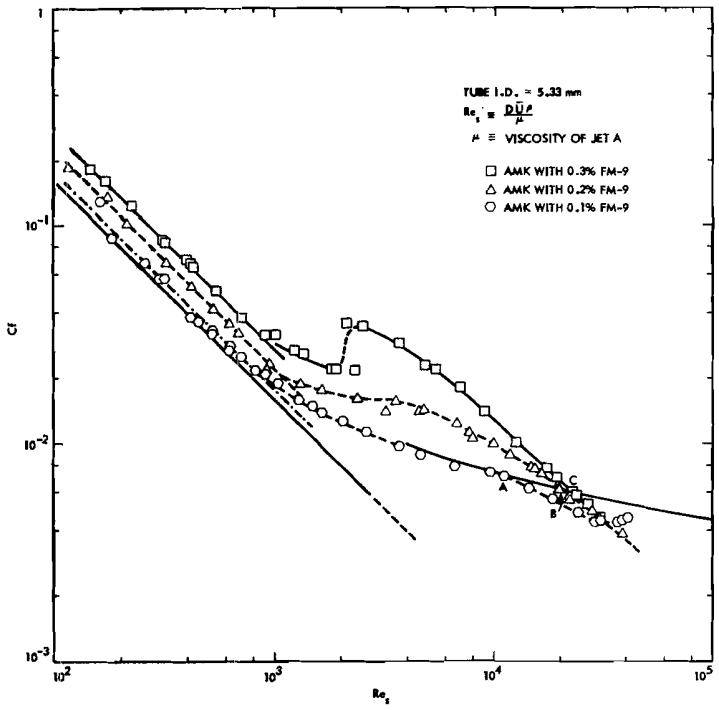

FIGURE 6. EFFECT OF THE FM-9 CONCENTRATION ON SKIN FRICTION; D = 5.33 MM, $\mu = \mu_{JET\ A}$

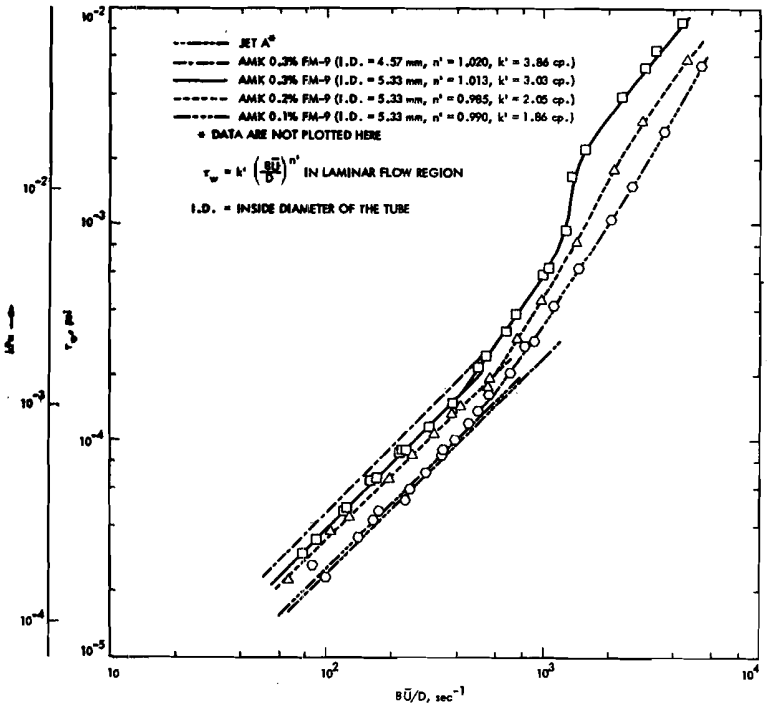

FIGURE 7. EFFECT OF THE FM-9 CONCENTRATION ON SKIN FRICTION; τ_w vs. $\dot{\gamma}_w$

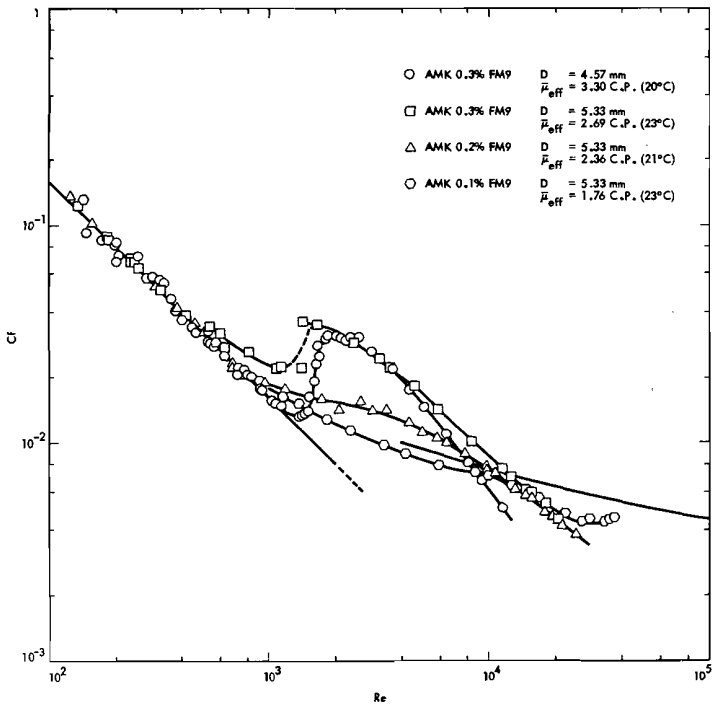

FIGUURE 8. EFFECT OF THE FM-9 CONCENTRATION OF SKIN FRICTION; $\mu = \bar{\mu}eff$

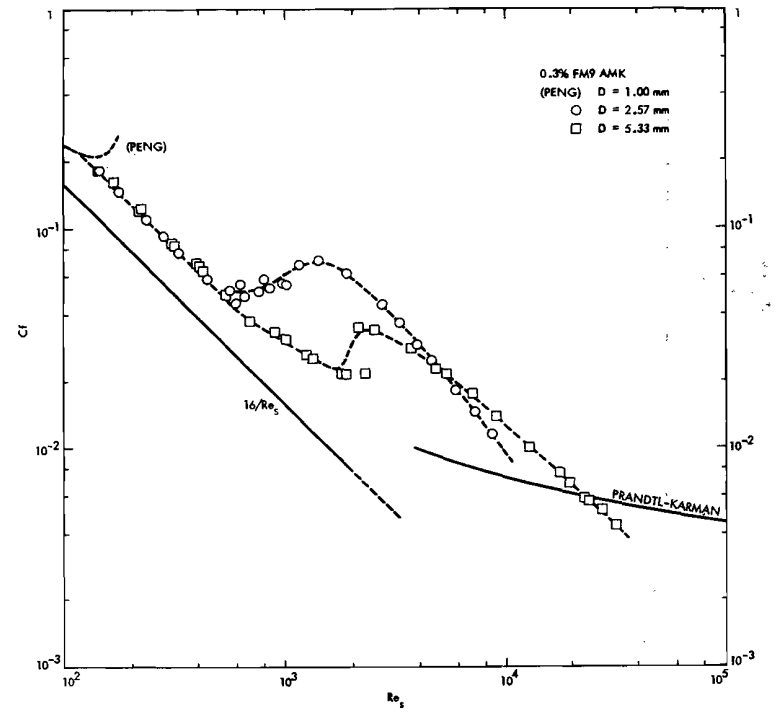

FIGURE 9. EFFECT OF THE TUBE SIZE ON SKIN FRICTION; D = 1.00, 2.57 and 5.33 MM, $\mu = {}^{\mu}$ JET A

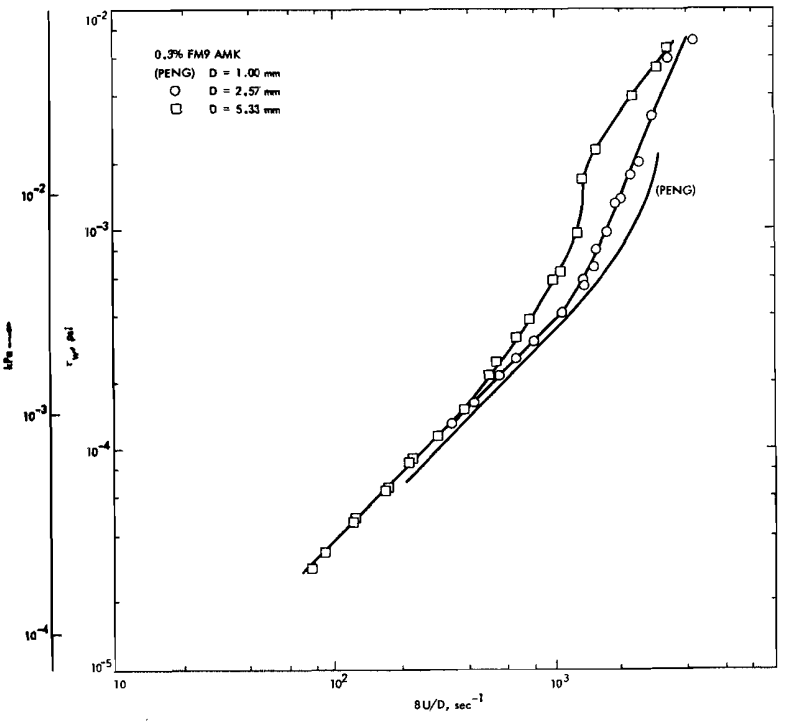

FIGURE 10. EFFECT OF THE TUBE SIZE ON SKIN FRICTION; τ_w vs. $\dot{\gamma}_w$

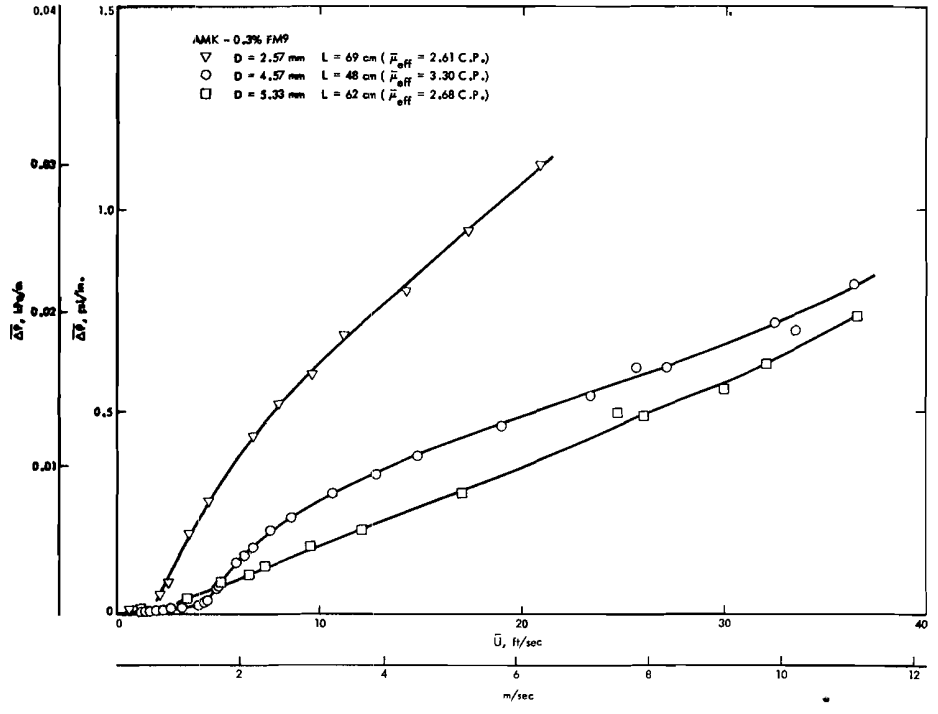

FIGURE 11. EFFECT OF THE TUBE SIZE ON PRESSURE DROP AT DIFFERENT FLOW RATES

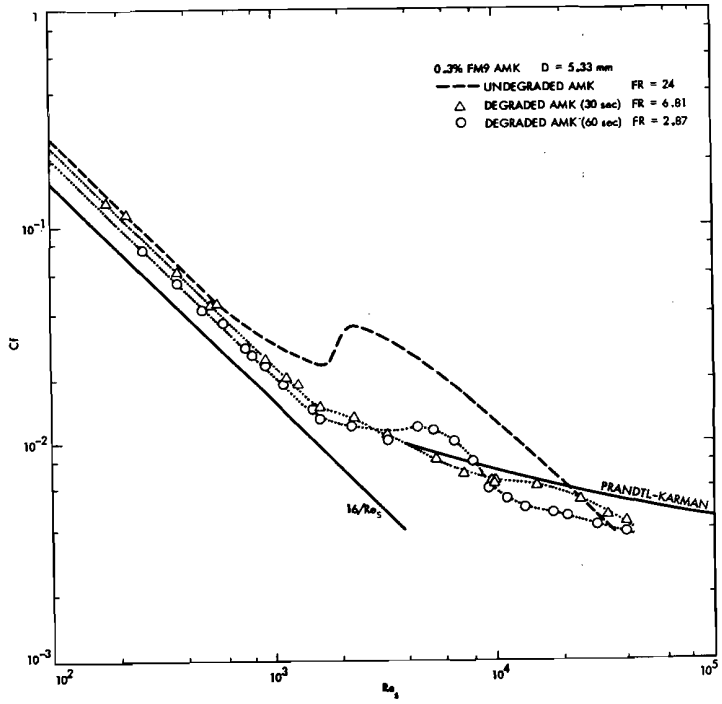

FIGURE 12. EFFECT OF THE RESTORATION LEVEL ON SKIN FRICTION; FR = 24, 6.81 AND 2.87, D = 5.33 MM, $\mu = \mu_{JET\ A}$

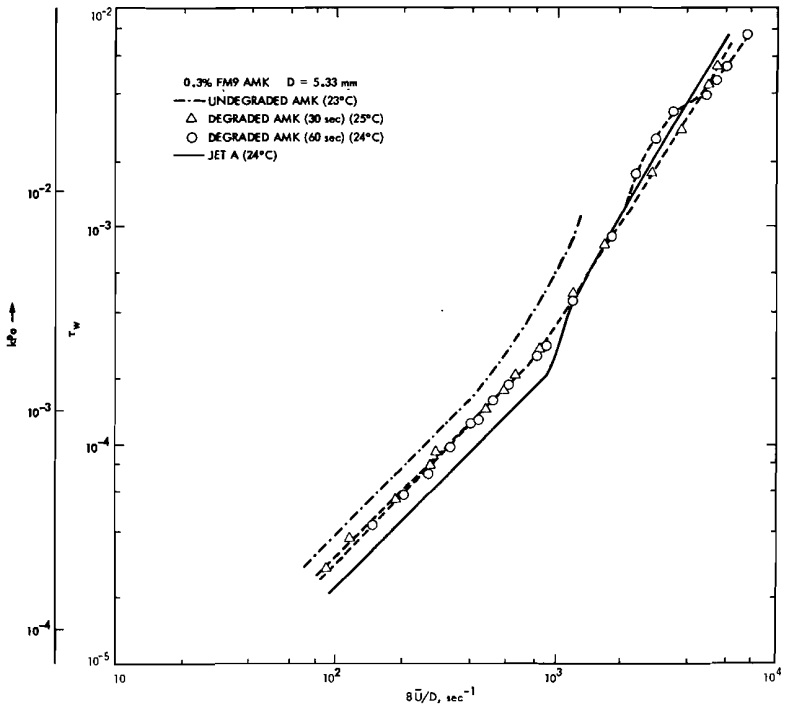

FIGURE 13. EFFECT OF THE RESTORATION LEVEL ON SKIN FRICTION; τ_w vs. $\dot{\gamma}_w$

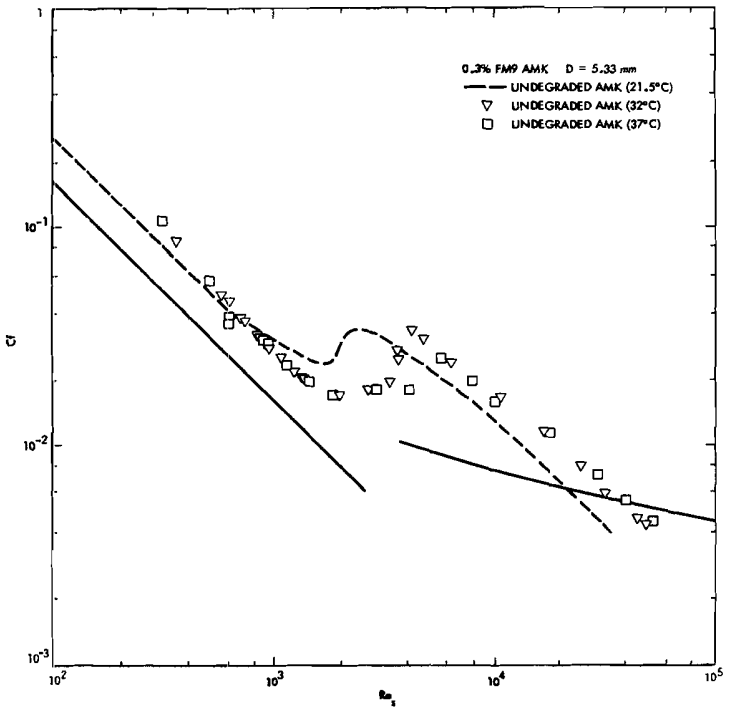

FIGURE 14. EFFECT OF THE FUEL TEMPERATURE ON SKIN FRICTION; T = 21.5, 32 AND 37° C, D = 5.33 MM, $\mu = \mu_{JET\ A}$

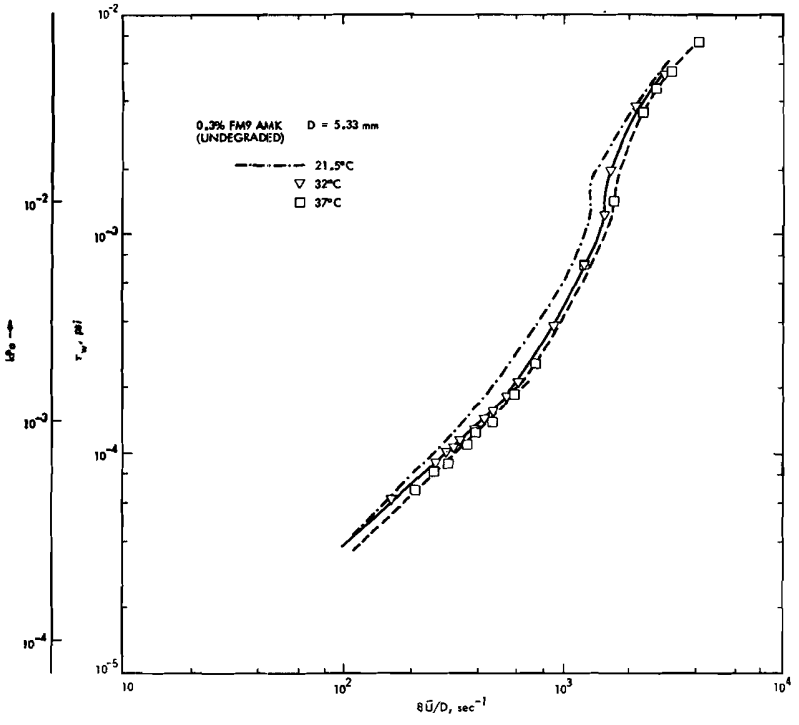

FIGURE 15. EFFECT OF THE FUEL TEMPERATURE ON SKIN FRICTION; τ_w vs. $\dot{\gamma}_w$

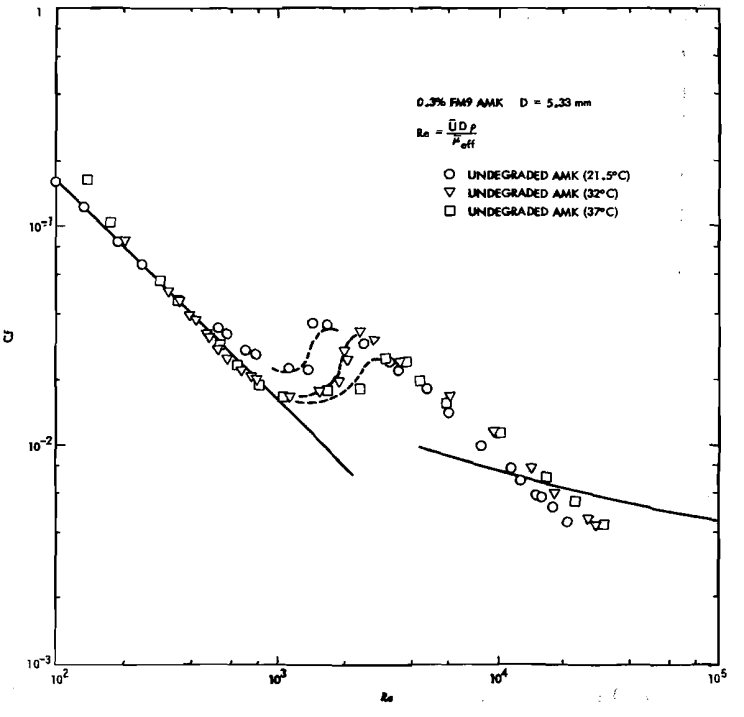

FIGURE 16. EFFECT OF THE FUEL TEMPERATURE ON SKIN FRICTION; $\mu = \bar{\mu}_{eff}$

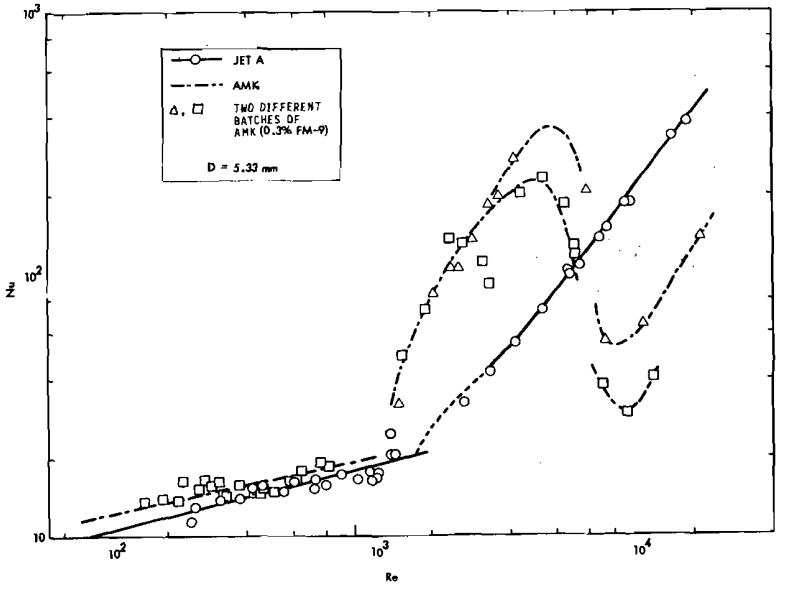

FIGURE 17. HEAT TRANSFER OF JET A AND 0.3% M-9 AMK; $Re = Re_b$, D = 5.33 MM

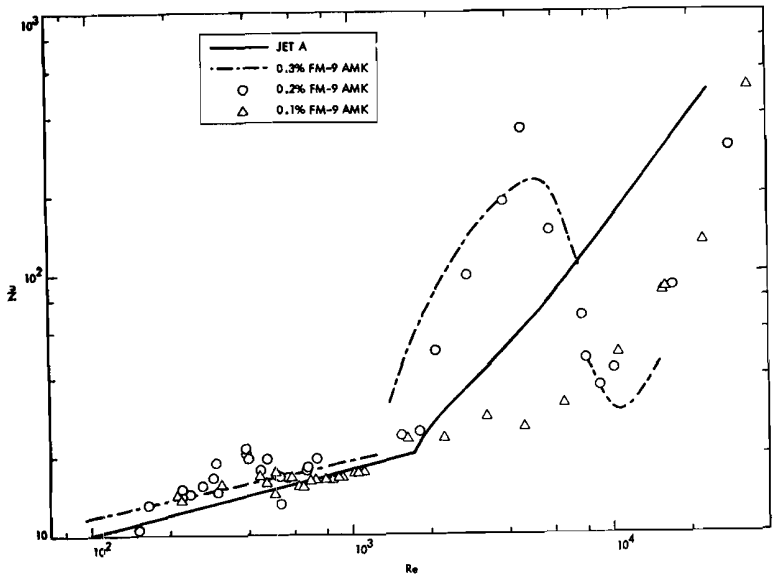

FIGURE 18. EFFECT OF THE FM-9 CONCENTRATION ON HEAT TRANSFER; D = 5.33 MM

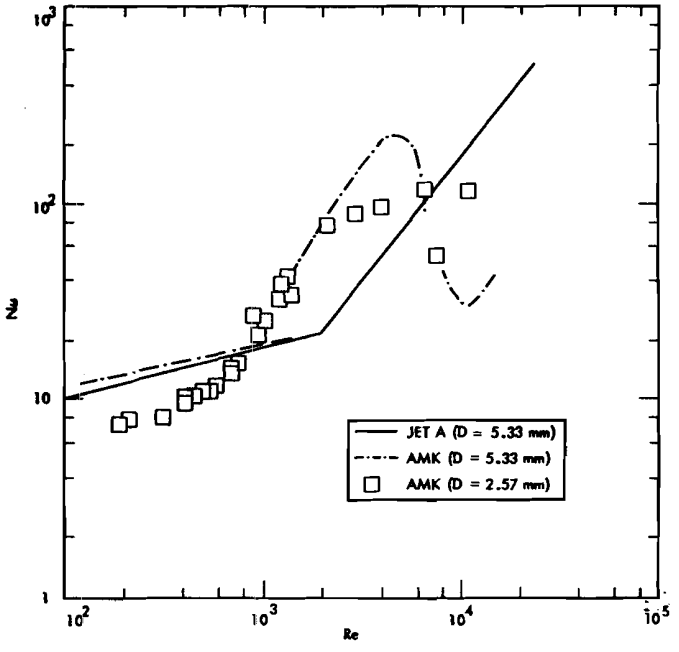

FIGURE 19. EFFECT OF THE TUBE SIZE ON HEAT TRANSFER; D = 2.57 & 5.33 MM FOR 0.3% FM-9 AMK

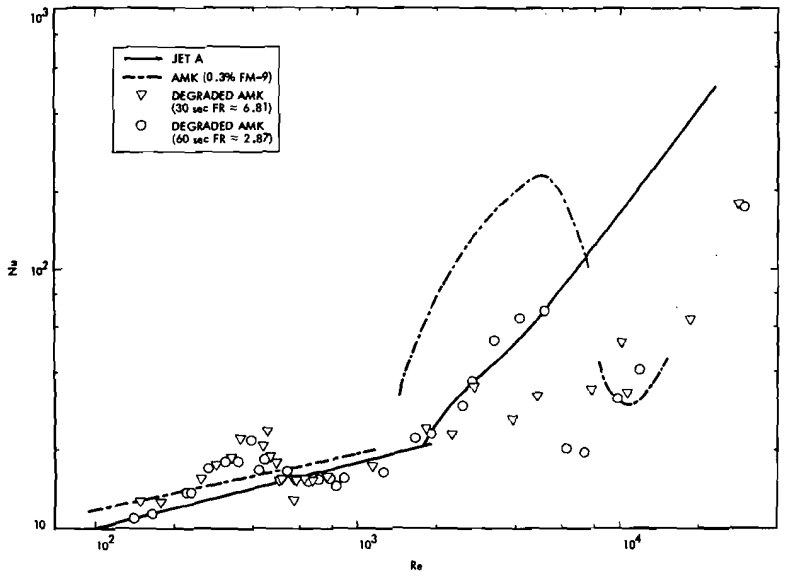

FIGURE 20. EFFECT OF THE RESTORATION LEVEL ON HEAT TRANSFER; D = 5.33 MM

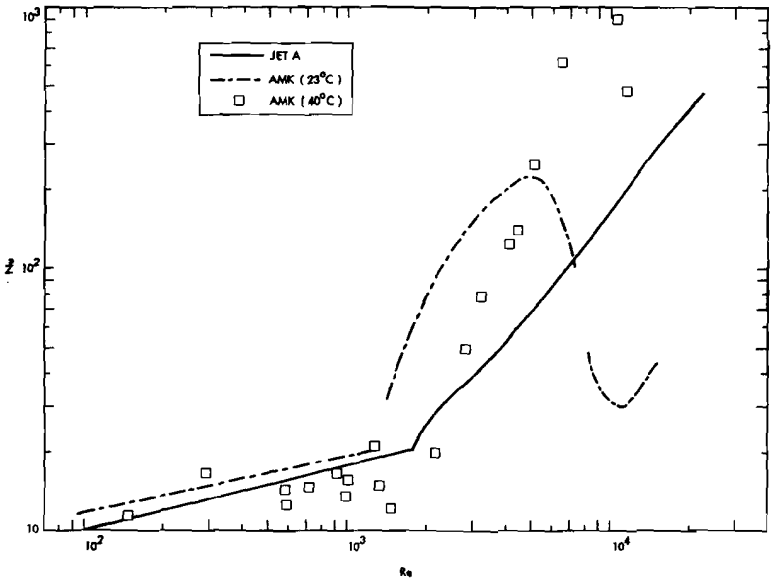

FIGURE 21. EFFECT OF THE FUEL TEMPERATURE ON HEAT TRANSFER; D = 5.33 MM

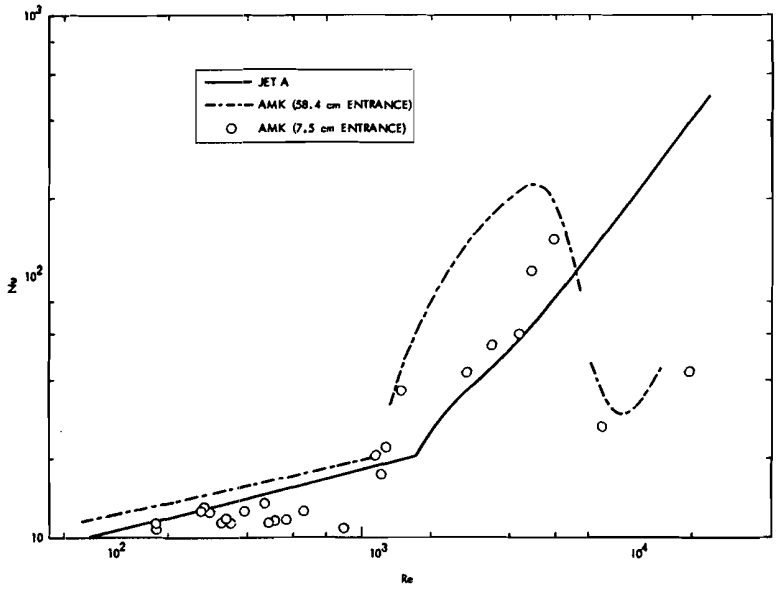

FIGURE 22. ENTRANCE EFFECT ON HEAT TRANSFER; D = 5.33 MM

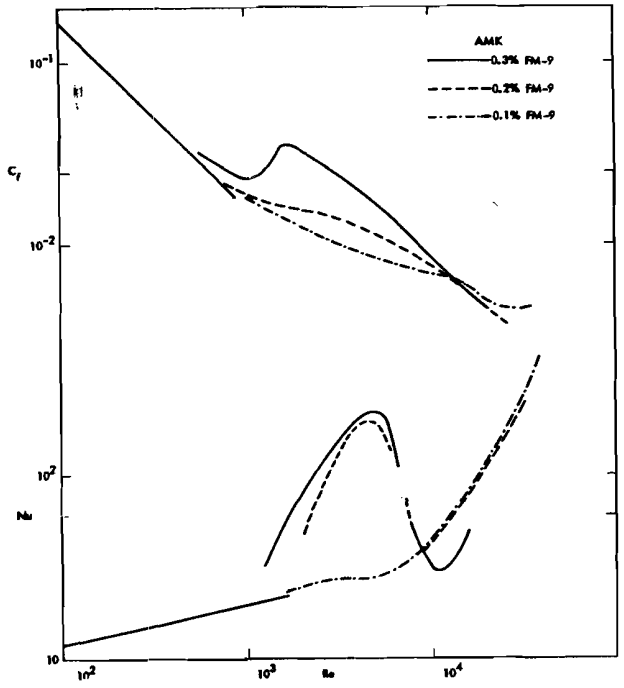

FIGURE 23. CORRELATION BETWEEN SKIN FRICTION AND HEAT TRANSFER

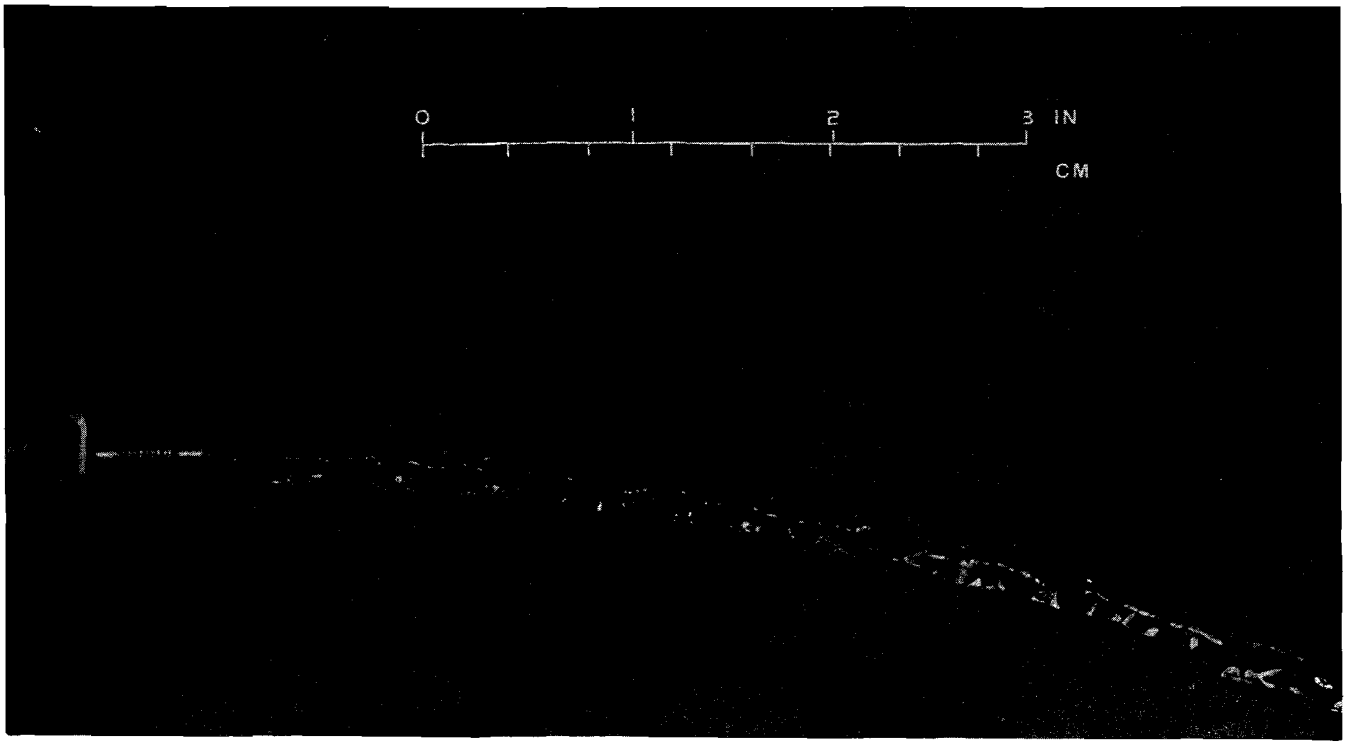

a. JET A, $Re_S = 2.6 \times 10^3$

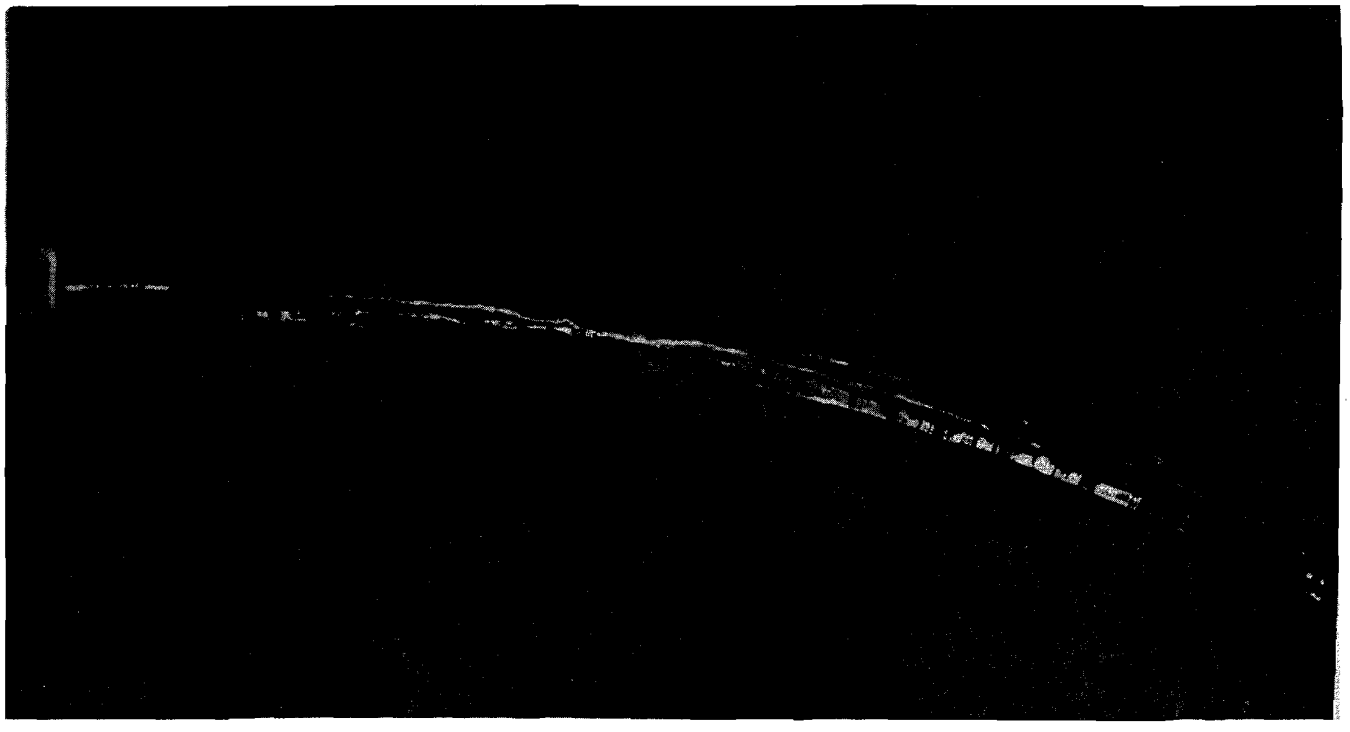

b. AMK, $Re_S = 2.8 \times 10^3$

FIGURE 24 VISUALIZATION OF FREE FUEL JET SHOWING THE DIFFERENCE IN FLOW BEHAVIOR

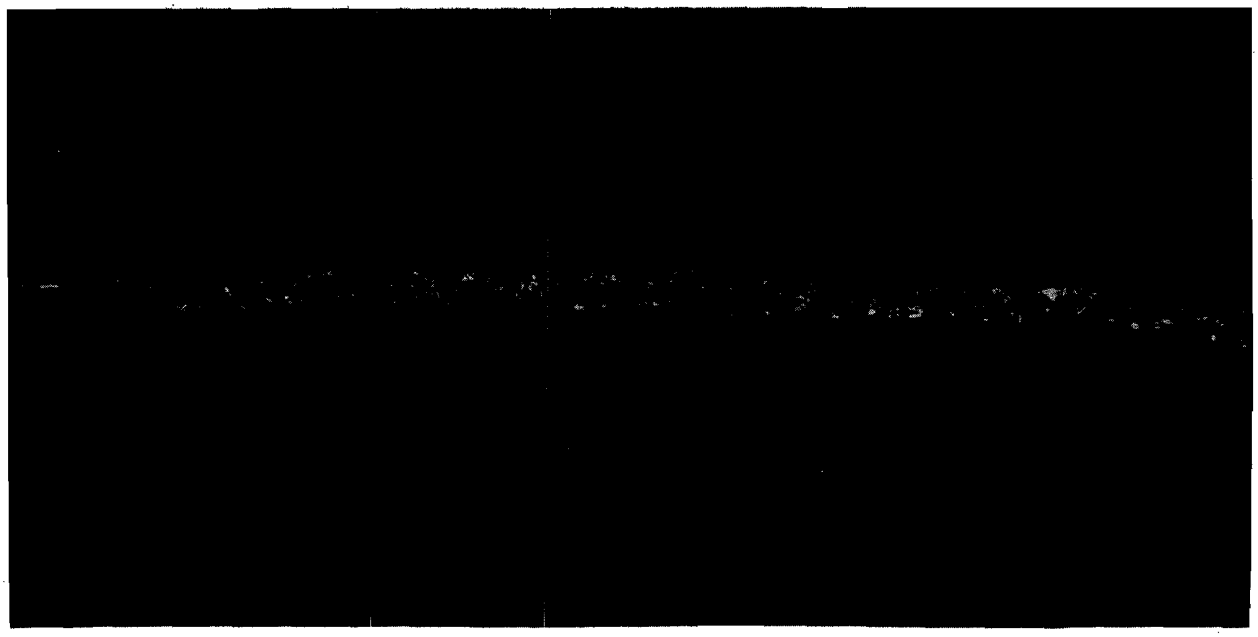

a. JET A, $Re_s = 5.3 \times 10^3$

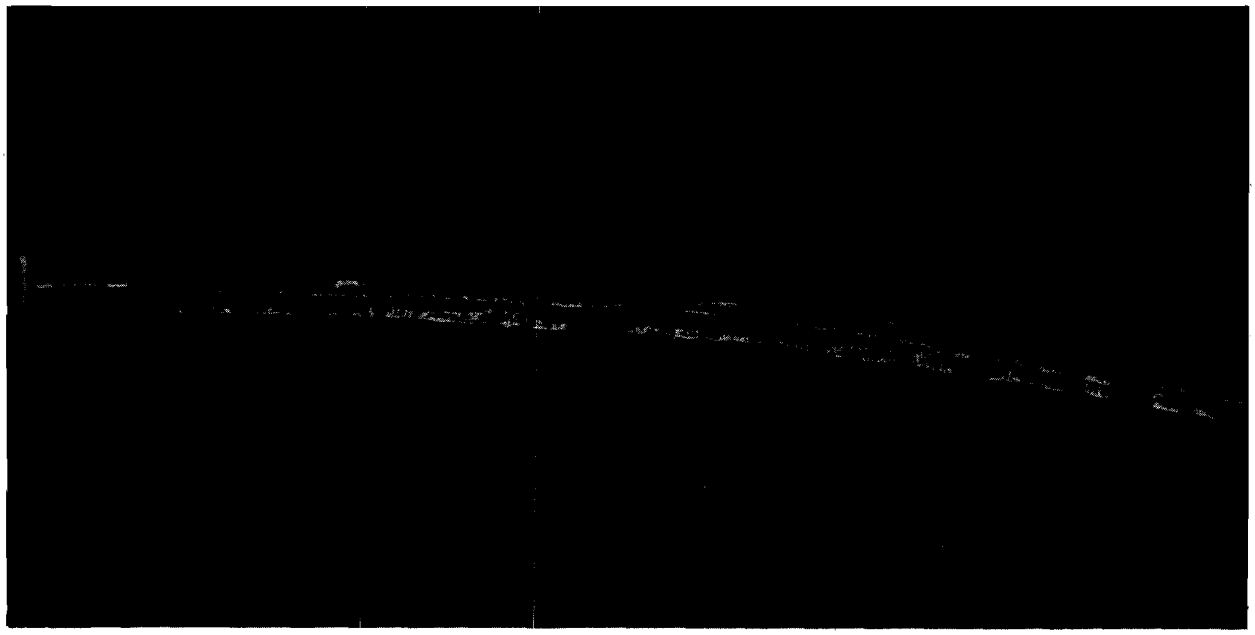

b. AMK, $Re_s = 5.2 \times 10^3$

FIGURE 25 VISUALIZATION OF FREE FUEL JET SHOWING THE DIFFERENCE IN FLOW BEHAVIOR

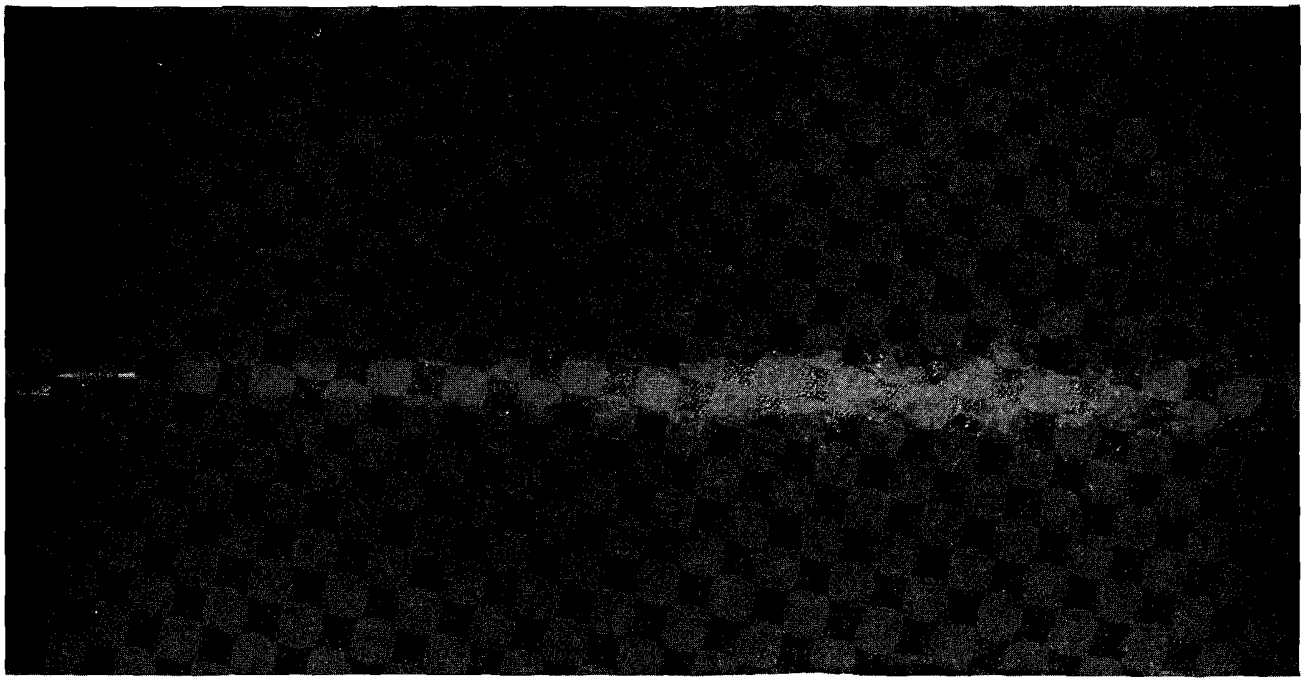

a. JET A, $Re_S = 3.5 \times 10^4$

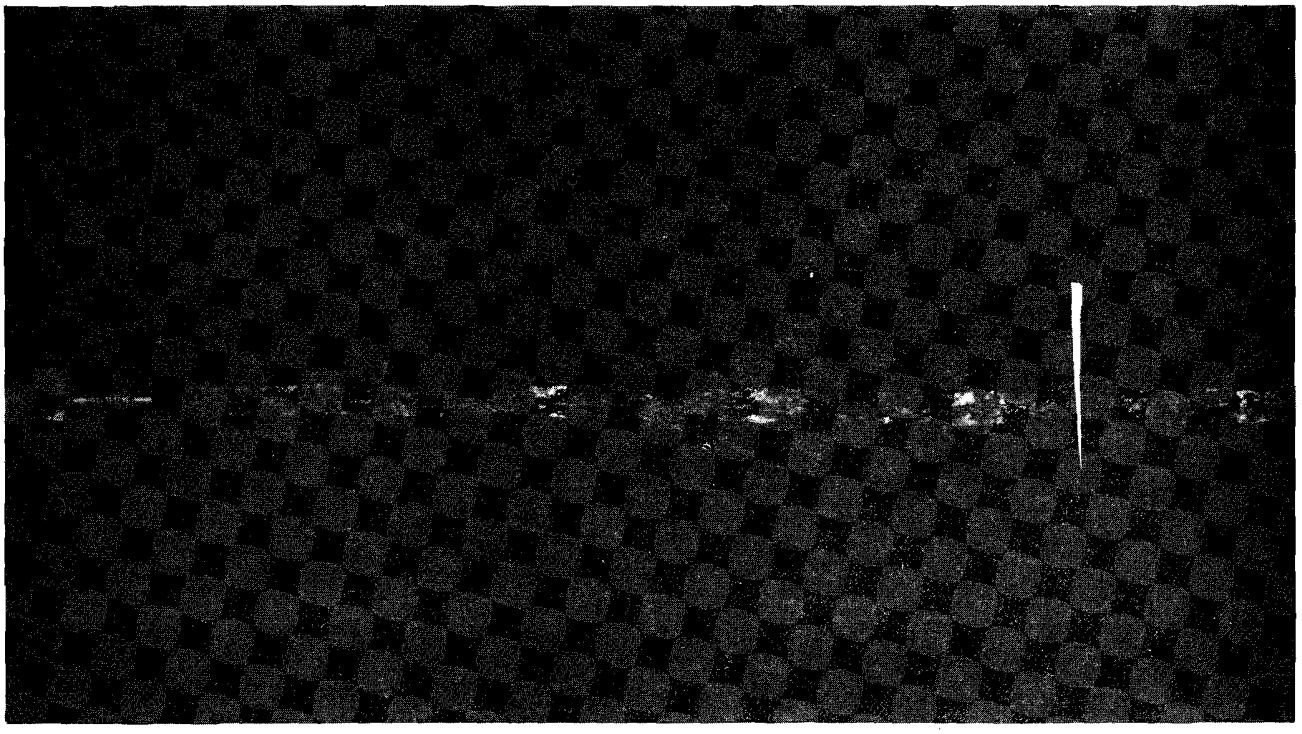

b. AMK, $Re_S = 3.0 \times 10^4$

FIGURE 26 VISUALIZATION OF FREE FUEL JET SHOWING THE DIFFERENCE IN FLOW BEHAVIOR

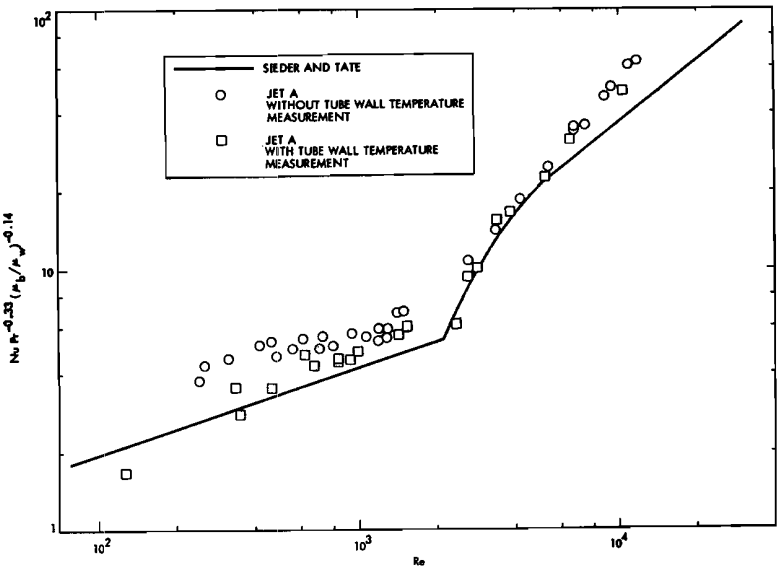

FIGURE 27. HEAT TRANSFER MEASUREMENTS OF JET A WITH AND WITHOUT WALL TEMPERATURE MEASUREMENT; D = 5.33 MM

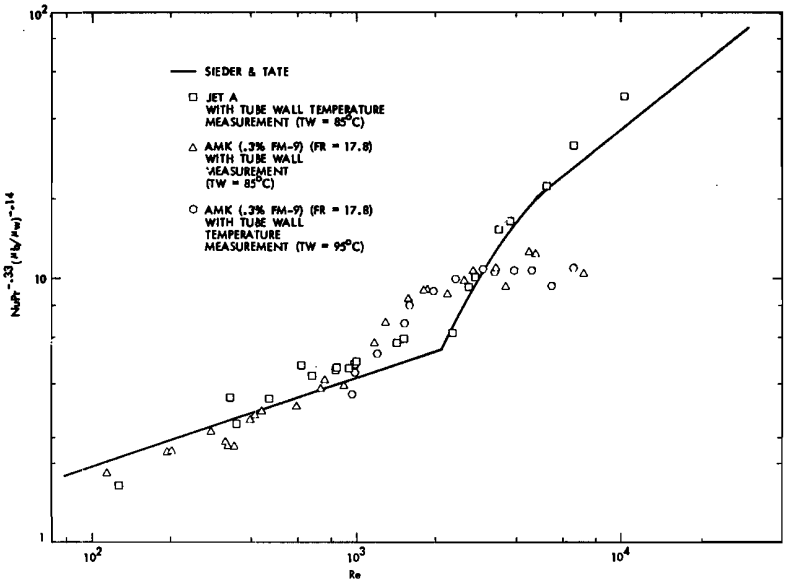

FIGURE 28. HEAT TRANSFER MEASUREMENTS OF JET A AND DEGRADED AMK WITH WALL TEMPERATURE MEASUREMENT; D = 5.33 MM

APPENDIX A: COMPUTATION OF THE HEAT TRANSFER COEFFICIENT

To calculate the heat transfer coefficient, h_f, between the wall of the tube and the jet fuel:

$$\dot{q} = \dot{m}\, C_{P_b}\, (T_2 - T_1) \qquad \text{A.1}$$

$$= \overline{U}_f A_f \quad \Delta\overline{T}_m \qquad \text{A.2}$$

where

$$\Delta T_m = \frac{(T_3 - T_1) - (T_4 - T_2)}{\ln \frac{T_3 - T_1}{T_4 - T_2}} \qquad \text{A.3}$$

Since the difference between T3 and T4 is less than 1° C in the experiment, mean temperature T_w has been used for ΔT_m, such that:

$$\Delta T_m = \frac{T_2 - T_1}{\ln \frac{T_w - T_1}{T_w - T_2}} \qquad \text{A.3a}$$

also

$$\frac{1}{u_f} = \frac{1}{h_f} + \frac{t\, dA_f}{k_t dA_t} + \frac{dA_f}{h_s dA_w}$$

$$= \frac{1}{h_f} + \frac{t}{k_t \frac{r_m}{r_i}} + \frac{1}{h_w \frac{r_o}{r_i}} \qquad \text{A.4}$$

The values of the second term are as follows:

$$\frac{t}{k_t \frac{r_m}{r_i}} = 3.92 \times 10^{-5} \ \frac{\text{hr m° C}}{\text{kg-cal}}$$

and

$$= 2.31 \times 10^{-5} \ \frac{\text{hr m° C}}{\text{kg-cal}}$$

for 5.33 mm and 2.57 mm I.D. tubes respectively. Since the value is small when compared to other terms, this term is neglected in the following calculation.

For h_w, which is the heat transfer coefficient between the tube water and the water in the annular space, Davis's equation (reference 24),

$$\frac{h_w D_1}{k_w} = 0.038 \left(\frac{D_1 \overline{U}\rho}{\mu}\right)_b^{0.8} \left(\frac{Cp\mu}{k}\right)_b^{.33} \left(\frac{\mu_b}{\mu_w}\right)^{.14} \left(\frac{D_2}{D_1}\right)^{.15}, \qquad \text{A.5}$$

is used.

The handbook values for the specific heat and thermal conductivity of kerosene, being used for all calculations, are:

$$k_f = 3.348 \times 10^{-4} \text{ cal/s cm}^\circ \text{ K}$$

$$C_p = 4.96 \times 10^{2} \text{ cal/kg}^\circ \text{ K}$$

When tube surface temperatures T_5 and T_6 are used, equation A.3 and A.4 will be changed to

$$Tm = \frac{(T_5 - T_1) - (T_6 - T_2)}{\ln \frac{T_5 - T_1}{T_6 - T_2}} \qquad \text{A.6}$$

and

$$\frac{1}{u_f} = \frac{1}{h_f} + \frac{t}{k_t \frac{r_m}{r_i}} \qquad \text{A.7}$$

respectively.

Hence, h_f can be calculated directly from the experiments. This experimental setup and measurement has been used and has yielded more accurate results.

APPENDIX B: DETAILS OF THE EXPERIMENTAL SETUP

TUBE O.D. (mm)	TUBE I.D. (mm)	$\frac{H_1}{D}$	$\frac{H_2}{D}$	$\frac{S_1}{D}$	$\frac{S_2}{D}$	DISCUSSION SECTIONS
1.59	.89	-	-	-	-	
3.18	2.57	-	-	230	290	3.1.3
		230	180	200	290	3.2.3
6.35	5.33	-	-	110	120	3.1.1, 3.1.2, 3.1.4, 3.1.5
		110	86	95	120	3.2.1, 3.2.2, 3.2.4, 3.2.5
		14	86	0	120	3.2.6

D = Inside Diameter

Pressure hole size = .66 mm

Heat Exchanger Outer Shell Size: O.D. = 6.03 cm
I.D. = 5.25 cm

APPENDIX C. OPERATING PROCEDURES FOR QUALITY CONTROL METHODS

JPL OPERATING PROCEDURE FOR FILTER TEST

1. Type of filter used: 12μm polycarbonate membrane (dia. 47mm.)
2. Make sure filter apparatus is clean (see the attached description of filter screen device.)
3. Place single membrane on filter plate; make sure it is placed flush against the surface to avoid leakage.
4. Attach plate to apparatus and secure clamps; tighten all screws evenly to insure equal pressure distribution.
5. Place rubber stopper in bottom hole.
6. Tilt apparatus and pour sample slowly down the side of tube. Do not let the sample hit the bottom directly.
7. Once tube is about 3/4 filled, return it to vertical, add sample to overflow into gallery.
8. Wait 30 seconds before removing rubber stopper.
9. Record time between time marks.
10. Dismantle and discard used filter--replace filter and repeat procedure.
11. If 17μm SS Dutch weave filter is used the filter can be reused (10-15 times), after the following cleaning procedure.
    a) Sonicate for 30 seconds in Jet A fuel.
    b) Sonicate for 30 seconds in acetone.
    c) Sonicate for 10 seconds in fresh Jet A fuel.
12. The filter is stored in Jet A fuel.

JPL OPERATING PROCEDURE FOR ICI CUP TEST

Cleaning Procedure:

1. Place cup in Jet A--fill cup about halfway with Jet A.
2. Sonicate for 30 seconds in Jet A fuel; power rating at 7.
3. Blow until dry with 25 psi nitrogen (1/4" hose). It is important that the area around the hole, both inside and out, is completely dry and free of particles.

Operating Procedure:

1. Suspend cup inside ring on ring stand; allow enough room below cup to permit introduction of graduated cylinder (preferably 10 cc).
2. Place finger over the hole, tilt cup slightly to one side. Pour in fuel sample allowing fuel to run down the sides of the cup rather than hitting the bottom directly.
3. Let fuel overflow into gallery.
4. Once cup is full, allow 30 seconds before releasing finger (fuel relaxation time).
5. Release finger at 30-second mark, recovering fuel in beaker beneath hole. Let the cup drain for another 30 seconds.
6. Again at the 2nd 30-second mark, simultaneously slide graduated cylinder in place of beaker--collect for another 30 seconds then remove graduated cylinder and replace beaker.
7. Record amount of fluid collected.
8. Discard collected material and repeat cleaning procedure.
9. After cleaning, the cup is stored in Jet A.

DESCRIPTION OF FILTER SCREEN DEVICE

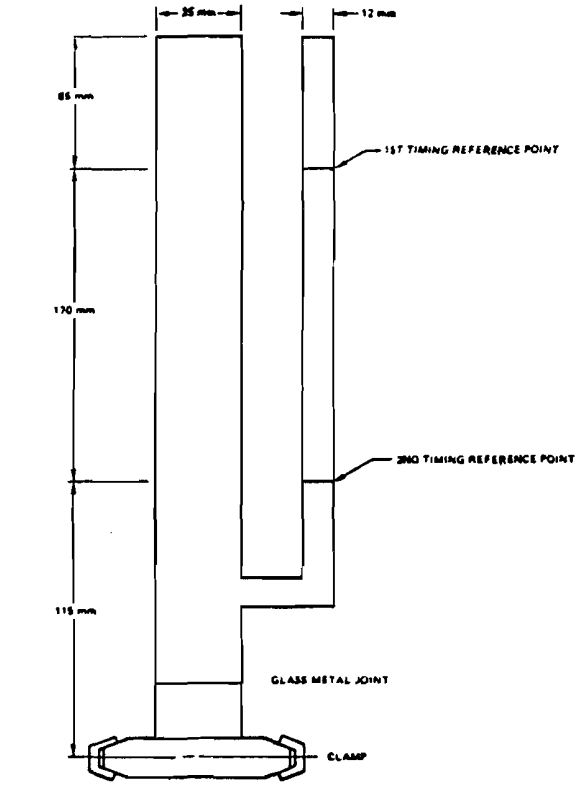

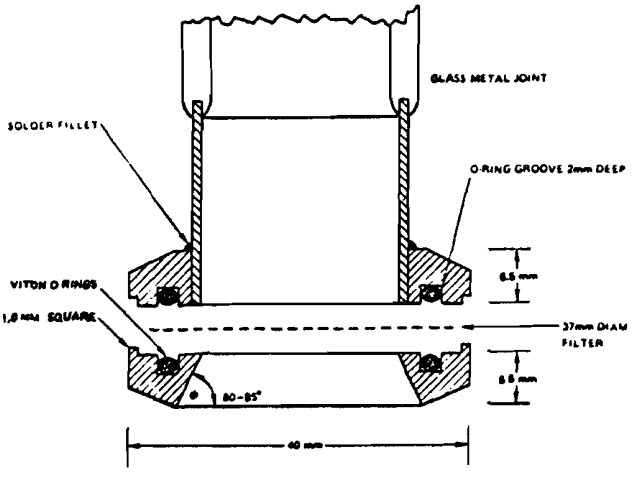

☆U.S. GOVERNMENT PRINTING OFFICE: 1982—505-067/35